Master of Science

거친 알루미나 기판 위에서 성장한 나노 구조화된 Ag(island shape) 위에 부착된 Pt/Pd Bimetal의 빠른 수소화과 탈수소화.

Fast hydrogenation and dehydrogenation of Pt/Pd bimetal decorated over nano structured Ag islands grown on rough alumina substrate

The Graduate School of the University of Ulsan

School of Electrical Engineering

Md Habibur Rahaman

Fast hydrogenation and dehydrogenation of Pt/Pd bimetal decorated over nano structured Ag islands grown on rough alumina substrate

Supervisor: Prof. Hyeon Cheol Kim

A Master's Thesis

Submitted to
the Graduate School of the University of Ulsan
in partial fulfillment of the requirements
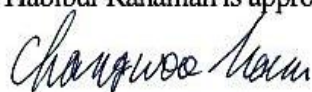for the degree of

Master of Science

by

Md Habibur Rahaman

School of Electrical Engineering
Ulsan, Republic of Korea
December 2018

Fast hydrogenation and dehydrogenation of Pt/Pd bimetal decorated over nano structured Ag islands grown on rough alumina substrate

This certifies that the Master's Thesis
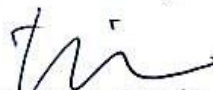of Md Habibur Rahaman is approved.

Prof. Dr. Chang-Woo Nam

Committee Chair, Dr.

Prof. Dr. Hyeon-Cheol Kim

Committee Member, Dr.

Prof. Dr. Tae-Woo Kim

Committee Member, Dr.

School of Electrical Engineering

Ulsan, Republic of Korea

December 2018

ACKNOWLEDGEMENT

ABSTRACT

In this thesis, the author developed and analyzed the fabrication and characterization of the hydrogenation and dehydrogenation in Pt/Pd bimetal decorated over Ag nanoislands grown over alumina substrate. The Ag nanoislands development on alumina substrate, formation of uniform Pt/Pd bimetal and their gas absorbing and desorbing performance along with theoretical investigations at various conditions such as different gas concentrations, different temperature have been undertaken.

A thermally annealed surface diffusion effects on the morphology of Ag nanoislands were analyzed with different morphological conditions. The author explored the catalytic bimetal nano structural effects on the surface charge density and the interfacial interactions with well-shaped Ag metal nanoislands. Several materials characterizations such as x-ray diffractions, atomic force microscopy, scanning electron microscopy, EDS analysis, photoluminescence effects, x-ray photo spectroscopy along with bimetals computational simulation were employed to confirm the catalytic properties of the as prepared structure toward hydrogen gas.

The morphology of Ag nanoislands was optimized by RF magnetron sputtering and rapid thermal annealing process. Later, Pt/Pd bimetal (10/10) nm were deposited by RF magnetron sputtering on the nanostructured Ag islands. After the surface morphological optimization of Ag nanoislands, the resultant structure Pt/Pd@Ag nanoislands at alumina showed a fast and enhanced hydrogenation and dehydrogenation (20/25 sec), response magnitude of 2.3% (10000 ppm), and a broad detection range of 500 ppm to 40000 ppm at the operating temperature of 120°C. The superior hydrogenation and dehydrogenation features can be attributed to the hydrogen induced changes in the work function of Pt/Pd bimetal which enhances the columb scattering of percolated Pt/Pd@Ag nanoislands. More importantly, the

atomic arrangements and synergetic effects of complex metal alloy interfacial structure on Ag nanoisland, supported by rough alumina substrate incorporates vital role in accelerating the H_2 absorption and desorption properties.

For the future hydrogenation and dehydrogenation related applications, this research provides a new technique to explore by using the simple nanostructure based model.

TABLE OF CONTENTS

LIST OF FIGURES

LIST OF TABLES

CHAPTER1: INTRODUCTION

The purpose of this chapter is to illustrate a framework and introduction of the research work. Whole chapter is divided among three sections which are research motivations, objective, and thesis organization

1.1. Motivation

For decades, being one of the most extensively used gas, hydrogen is attracting to create a great economy in the fields of clean energy transportation and system [1], petroleum products refining [2, 3], fuel source [3], power generation [2], energy storage [4]. However, since the use of hydrogen is associated with various safety related issues as it's a colorless and odorless based gas along with a explosion property over the concentration of 4% [5]. Thus, it necessitates an accurate system, by which the hydrogenation phenomenon can be accurately measured within very short time in different conditions [5]. Recently, numerous researches are performing for the smooth hydrogenation and dehydrogenation of various metal oxides system such as (In_2O_3, SnO_2, ZnO, TiO_2, WO_3) but their high temperature requirements increase the power consumption [6-8]. Furthermore, the slower response and recovery for the aforementioned metal oxides may hinder the safety issue. To address these issues, researchers deployed Pd (palladium) as a metal catalyst which has a high selectivity with a good absorption rate at lower temperature to hydrogen gas [9, 10]. However, a mechanical embrittlement and hysteresis effect at higher hydrogen concentration makes it unstable to maintain its sensing ability. Several kinds Pd nanostructures such as nanowires [11], nanochains [12], nanoflowers [13], nanotubes[14], nanocomposites [15] show improved results in terms of stability and power consumptions. Along with this nanostructure formation, combining with Pt (platinum) at nanoscale label further increases the hydrogenation and

dehydrogenation properties [16, 17]. However, these structures need complex fabrication process along with conductive graphene derivatives which might face some agglomeration effect. Thus, it is highly desirable to design a simple cost effective structure with highly catalytic Pt/Pd metal alloy for enhanced hydrogenation and dehydrogenation process. Ag is a cost effective and light weight metal which can provide a better catalytic interfacial alloy formation with Pd that has more solubility and permeability towards hydrogen gas [15, 17, 46]. However, only Pd-Ag alloy couldn't satisfy the fast hydrogenation and dehydrogenation process [15,17], more comprehensive findings are needed to optimize the catalytic properties.

In this present study, for the very first time, we are reporting the hydrogenation and dehydrogenation of nanosized Pt/Pd bimetal decorated over Ag nanoislands grown at alumina substrate. Thin Ag film was deposited by ultra-high vacuum RF magnetron sputtering followed by a rapid thermal annealing process for inducing the nanoislands morphological structure. Pt/Pd bimetal was also deposited by RF magnetron sputtering on the Ag nanoislands to form a capping layer. This nanostructured Ag islands morphology provides a higher interfacial alloy with catalytic bimetal of Pt/Pd. Furthermore, it is expected that, the islands structure would provide a percolated conductive pathway by increasing the connectivity with the bimetal at nanoscale level. The as fabricated structure was used as to observe the resistance change for detection for the hydrogenation and dehydrogenation process.

1.2. Objectives

This study reports the fast hydrogenation and dehydrogenation of ultra-thin discrete platinum/palladium (Pt/Pd) bimetal over Ag nanoislands grown on rough alumina substrate by RF sputtering technique. The morphology of Ag nanoislands was optimized by RF

magnetron sputtering and rapid thermal annealing process. Later, Pt/Pd bimetal (10/10) nm were deposited by RF magnetron sputtering on the nanostructured Ag islands. The objectives of this work are illustrated below

- ✓ Fast hydrogenation and dehydrogenation time

- ✓ Good sensitivity

- ✓ Wider detection range

- ✓ Linearity in large detection range (500 to 40000 ppm)

- ✓ Good repeatability in 10000 ppm

- ✓ Elevated temperature (120˚C)

- ✓ Light weight, small size

- ✓ Highly hydrophobic catalytic substrate.

For evaluating the hydrogenation and dehydrogenation properties, we optimized the Ag nanoislands structure and grew different nano sized Ag particles by varying the deposition conditions and applied rapid thermal annealing process to connect the particles by coalescence mechanism. This modified nanostructured particles after coalescence showed islands structure which later helps to utilize a percolated islands structure with an enhanced ohmic conduction. This percolating channel greatly supported to optimize the nanostructure of Pt/Pd bimetal to be deposited for hydrogen permeation and deportation. After that, Pt/Pd bimetal with high surface to volume ratio were deposited over the Ag nanoislands. Finally, we explored the hydrogenation and dehydrogenation by applying a bias voltage in realistic

gas environment, in which fast response and recovery, changes in hydrogen concentrations were found.

1.3. Thesis organization

This thesis is structured to illustrate the theoretical and experimental presentation of the research conducted by the author. In detail, the fabrications, theoretical investigation along with characterization of bimetallic Pt/Pd at Ag nanoislands over alumina substrate as hydrogenation and dehydrogenation model were analyzed. Furthermore, fast evaluation of the hydrogenation and dehydrogenation of the as prepared model opens up the potentialities of hydrogen sensor to be used in safety application with more improvement such as stability and selectivity. The thesis is organized as follows;

- Chapter 1 Introduction

  A short introduction and motivation behind the study, and overall works contents are illustrated in this section.

- Chapter 2 Literature review and background

  Backgrounds of this study along with nanomaterials familiarization and the state of the art are discussed elaborately in this section

- Chapter 3 Experimental procedures and evolution

  All experiments steps and device fabrications processes along with experimental tools and their processes were explained elaborately in this section

- Chapter 4 Hydrogenation and dehydrogenation performance analysis of

    Pt/Pd@Ag nanoislands decorated over alumina

- Chapter 5 Hydrogenation and dehydrogenation performance analysis of Pt/Pd@Ag

    nanoislands deposited over alumina were analysed and investigated in this

    section

- Chapter 6 Conclusions and future work

    The overall outcomes of this research are summarized in this section.
    Furthermore, some suggestions for the improvement of this model was
    also analyzed for the future work related to this research are discussed

CHAPTER 2. LITERATURE AND BACKGROUND REVIEW

2.1 Overview on the necessity of hydrogen economy

In recent years, hydrogen gas has been widely used in several applications such as, fuel cell for generating electricity, refining of petroleum products,, propellant for spaceships, powering cars with the envisioning of transforming fossil-fuel based economy to a renewable energy based [18]. To cope up these huge demands in commercial applications, huge amount of hydrogen are being produced [19]. An amount of 57 million metric tons of hydrogen with a growth rate of 10% per year were recorded at 2004 [20]. However, one of the roadblocks to the huge uses of hydrogen as a renewable fuel is hydrogen storage specifically for on board vehicles [21]. Hydrogen gas is highly flammable and explosive (over 40000 ppm in air) that increases the necessity to design and fabricate very sensitive and fast hydrogen detection system. A highly accurate hydrogenation and dehydrogenation system can provide the measurement of wider ranges of concentrations during hydrogen handling, production, storage and transportation [18-21]. Detection of hydrogen content in a mixed gas system during reaction need to respond accurately and the high frequency monitoring in the power generation from fuel cell can be utilized with fast hydrogenation and dehydrogenation system appropriately [22].

Fig 2-1. Hydrogen economy [18-21]

2.2 Requirements for hydrogen detection system

- ✓ Explosion sustainable device design

- ✓ Low power consumption

- ✓ Higher level of sensitivity with accuracy

- ✓ Low noise based stable signal with faster hydrogenation and dehydrogenation property

- ✓ Less hysteresis and highly repeatable

- ✓ Low cost, compact design with simple maintenance and operations.
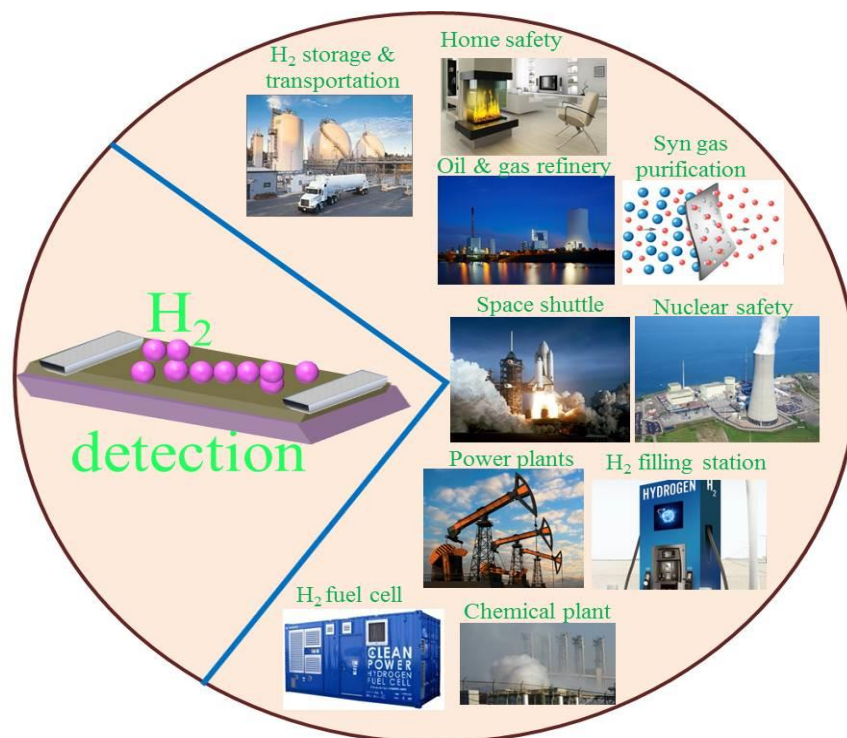
Fig. 2-2. Hydrogen detection applications [1-15]

2.3 Nanomaterials based hydrogen detection

Nanomaterials have been extensively studied for their diverse applications in chemical industry, medical sectors, food technology, national defense and our daily life. [54, 22]. A rapid advancement in the nanotechnology is taking the world's technology to a new height. High performance electronics devices and sensors are made by complex nanomaterials engineering. These nanomaterials include, metal oxide, carbon materials, 2D materials, ceramic materials etc. Among these, nanostructured catalytic metals and metal oxide semiconductor materials are being studied monumentally for their interaction with several gases in the environment. [2, 23]. Easy fabrication and intriguing nano sized effects on their physical and chemical properties made them favorable to study and research. ZnO, SnO2, Wo3 and TiO2 have catalytic effects toward hydrogen molecules but a higher power consumption (temp more than 400°C) for operating condition is needed. For improved

hydrogenation and dehydrogenation response at an elevated and comparatively less power consumption, the noble metals such as Pt, Pd, Au, Mg, Ni were used with metal oxides (ZnO, SnO2, Wo3, TiO2) and carbon materials (graphene, CNT) [24].

2.4 Catalytic nanomaterials based hydrogenation and dehydrogenation motivation

Palladium (Pd) has been extensively studied and researched as hydrogen sensing material with high sensitivity and selectivity. It's a fcc crystal structure based metal with an atomic weight of 106.42 and electronic confugration of $[Kr]4d^{10}$. At the time of physical absorption in hydrogenation , hydrogen molecules selectively absorbed in the Pd surface (fcc) and dissociated on the interstitial sites of Pd [25].

At the same time, surface conductivity of the Pd surface changes by the transition of solid solution of Pd/H (α-phase) to palladium hydride (ß-phase) which increases the lattice constant of Pd by 3.5% [26].
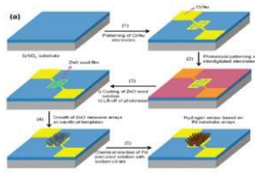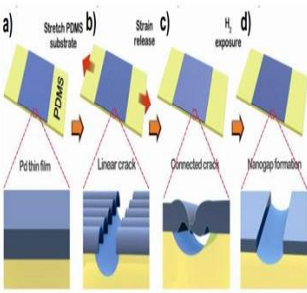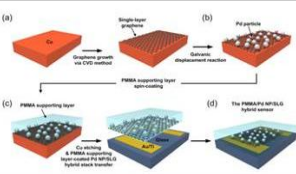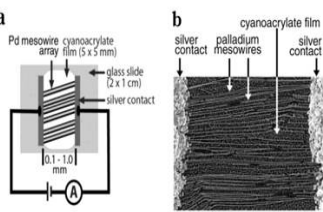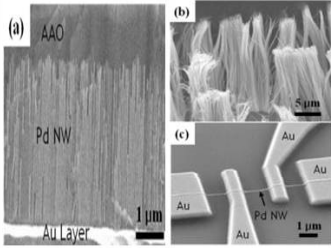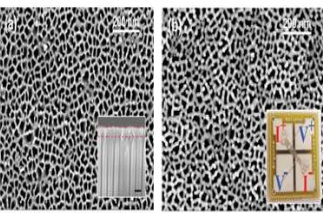
However, a hysteresis and repeatability problems occur onto the Pd thick films after numerous high concentration of (40000 ppm) hydrogen exposure [27]. This irreversible structural and morphological deformation eliminates the reusability and slows down the hydrogen atom desorption. To overcome these problems, progresses in the nanostructures and their device fabrication such as nanosized Pd deposited on the edges of graphite surface or nano channels of anodic alumina oxide (AAO) membranes showed enhanced hydrogenation proeprties. Nanostructured Pd wire electrodeposited by lithographically patterned, nano-patterns by electron beam lithography was reported for enhanced hydrogenation and dehydrogenation properties [28-34]

Inconvenient to reproduce, complex transfer process and non-industrial approach along with high fabrication cost hinders the potentiality of Pd nanowire electrodeposition on anodisc alumina oxide template [36].Novel Pd nanocube of ~50 nm was deposited uniformly over the edges of graphene layers by thack et al. which showed a response time of 2.8 minutes with 10% response magnitude at 10000 ppm hydrogen that is comparatively much slower. To lessen the fabrication complexity and more improved catalytic structure, we tried to study the Pd/Pt interfacial catalytic properties toward hydrogenation and dehydrogenation. Pt is a fcc crystal structure whose atomic weight is 195.078 with an electronic configuration [Xe] $4f^{14}5d^{9}6s^{1}$ [35, 36]. Jung et. al. showed that the catalytic activity of 6 nm e-beam evaporated Pt layer deposited on carbon nanotube toward hydrogen
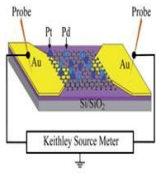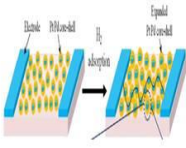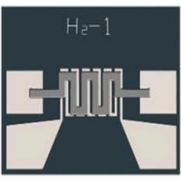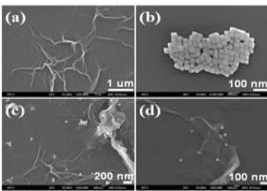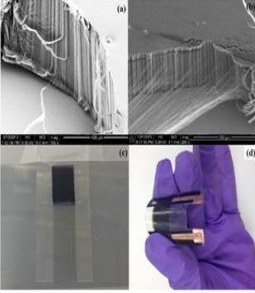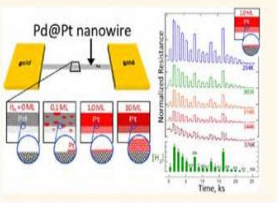
gas along with a wider response magnitude[37]. Although, the existence of oxygen on the sensing surface that hinders the sensing coverage was not analyzed. Although, a lithographically patterned electro deposited Pt/Pd nanowire was reported that shows a great detection range of 0.05 % to 5% at 303 K temperature however slower response and recovery time with a complex lithography process doesn't suit a mass production. Yang et. al. showed the uniform Pt/Pd nanoparticle distribution on GO nanoflakes with an enhanced sensing response of 50% at 10000 ppm hydrogen but a slower response and recovery time ~2/5 minutes at 150˚C [105]. A Pd core Pt shell on SAM monolayer structure for enhanced hydrogenation was reported by Uddin et. al. which shows a faster response time of 6 sec with 13% response magnitude at 150˚C [35].

The state of the art for Pt/Pd , Ag, GO based hydrogen sensor has been summarized in table 2.1.

Table. 2.1. Hydrogen sensor state of art [1-15]

Research institutes	Overview	Device structure	Disadvantages
KAIST S. Korea ACS nano, 2012	➢ Flexible Pd nanotube on sacrificial ZnO. ➢ Higher magnitude of response~67% at 10000 ppm ➢ Highly flexible and bendable		➢ Slower response time ~ 3 minute ➢ Effects of oxygen was not analyzed ➢ Complex fabrication process
Yonsei University S. Korea Angew. Chem 2012	➢ Pd/PDMS ➢ Mechanically induced nanogap ➢ Highly flexible ➢ Wider detection range		➢ Uncontrollable nanogap formation ➢ Adhesion between Pd/PDMS may get lower after several gas exposure ➢ Slower response recovery~>1 mint ➢ Effects of oxygen was not analyzed
Yonsei university S. Korea ACS Appl. Mater. Interfaces, 2014	➢ PMMA/Pd/Graphene ➢ High selectivity ➢ Flexible		➢ Slow response and recovery time ~ 2/6 mint ➢ Narrow range of sensitivity upto 2% of hydrogen concentration.
University of California, Irvine. USA Annal. Chem. 2002	➢ Pd mesowire in graphite defects ➢ Response time: 5 sec ➢ Wider sensing concentration range (1~10%) ➢ Slower recovery		➢ Inconvenient to reproducible. ➢ Complex transfer process ➢ High fabrication cost and non industrial approach ➢ Humid condition can affect the sensing outputs
Yonsei university S. korea. Nanotechnology, 2008	➢ Pd nano wires into nano channels of AAO by lithographically patterned electrodepposition ➢ Lift-off process ➢ Slower response and recovery (≥ 2 mint 10000 ppm)		➢ Electrical connection between the nano wires ➢ Complex transfer process ➢ Costly fabrication and non industrial approach ➢ Humid condition performance wasn't check
Northern Illinois university, USA, Nano letters, 2010	➢ Pd nano wire ≥ 10 nm was deposited on porous membrane ➢ Highly sensitive ➢ Cr was deposited to increase the surface conductivity ➢ Fast response and recovery (3~4 sec)		➢ Breakage of Pd nanowire above 10 nm ➢ Presence of Oxygen reduces the response

Research institutes	Overview	Device structure	Disadvantages
Donghua university China RSC advances 2016	➢ Pd-Pt-rGO ➢ Simple fabrication ➢ Higher response magnitude ~50 % ➢ Room temperature detection		➢ Slow response and recovery time ~5/8 minutes ➢ Unrepeatable device configuration
University of Ulsan S. Korea, IJHE 2016	➢ Pd@Pt core shell on SAM monolayer ➢ Wide limit of detection 0.01%~4% ➢ Effects of Pt shell ➢ Good selectivity ➢ Less humid conditions		➢ High temperature needed ➢ Difficulties in controlling core-shell structure ➢ Slower recovery ➢ Not suitable for mass production
University of Seoul, S. Korea, IJHE 2017	➢ Pd-Ag ➢ Good response magnitude~14.36% at 1000 ppm		➢ High temperature~153˚C ➢ Slower response / recovery ~120/ 150 sec
University of Ulsan, S. Korea, SNB 2014	➢ Pd nanocubes/Graphene ➢ Wide detection range ➢ Good response magnitude ~10 % at 10000 ppm hydrogen		➢ Slower response time and recover 2.8/5 minutes ➢ Effects of oxygen molecules weren't shown
University of Texas at Dallas USA ACS Appl. Mater. Interfaces 2015	➢ Pt-CNT ➢ Good response magnitude ~23% ➢ Faster response ~10 sec and recovery ~20 sec ➢ Wider detection ranges~ 3 to 33% ➢ Room temperature detection		➢ Effects of oxygen molecules weren't shown ➢ Non alignment of CNT can causes to reduce response
University of California USA ACS nano 2016	➢ Pd-Pt nanowire ➢ LPNE technique ➢ Low temperature detection ➢ Accelerated oxygen deportation at 100˚C		➢ Slower response recovery ➢ Complex fabrication process, non-industrial approach

CHAPTER 3. EXPERIMENTAL PROCEDURES AND EVALUATION

Several experimental steps were performed to grow Ag nanoislands on highly rough alumina substrate. The morphology of Ag nanoislands played an important role for enhancing the hydrogenation and dehydrogenation phenomenon along with good response magnitude. Furthermore, It increased the bimetal surface connectivity by higher surface to volume ratio in nanoscale level that eventually enhances the synergetic effects towards gas absorption and desorption. Although, an elevated temperature of 120˚C was needed to fully dehydrogenated at 25 sec, a faster hydrogenation time of 20 sec was measured for 10000 ppm hydrogen gas at 2.3 % response.

Ag nanoislands were synthesized by depositing an optimized layer of Ag thin film on alum mina substrate using ultra-high vacuum radio frequency magnetron sputtering, following a rapid thermal annealing process to induce surface diffusion phenomenon. Later, a bimetal structure of catalytic Pt/Pd was also deposited by RF magnetron sputtering technique.

3.1. Selection of substrate

Commercially available alumina substrate was used for its high roughness and hydrophobicity that enhance the nanostructured metal islands formation. First, a 10/5 mm^2 sized alumina substrate were taken and cleaned in methanol, isopropanol, and deionized (DI) water by ultra-sonication and dried with nitrogen gas, followed by heating in a hot-plate at 150˚C.

Before developing Ag nanoislands on alumina substrate, Ag was sputtered on alumina substrate by RF magnetron sputtering.
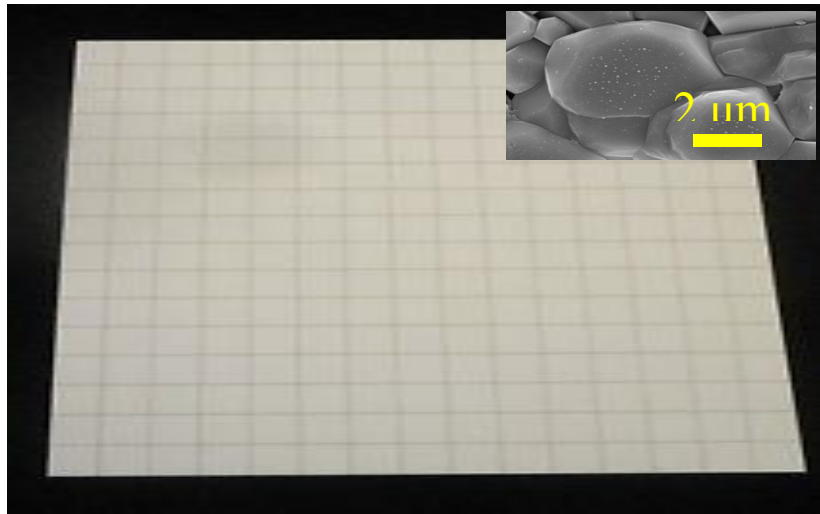
Fig. 3-1 Optical images of alumina substrate, inset showing rough alumina substrate

Different sizes of Ag nanoparticle were deposited by varying the deposition condition of RF magnetron sputtering. To perform the experiment, a highly pure Ag target of (99.999% purity) was used and a distance of 7cm was maintained between the substrate and target in sputtering chamber.
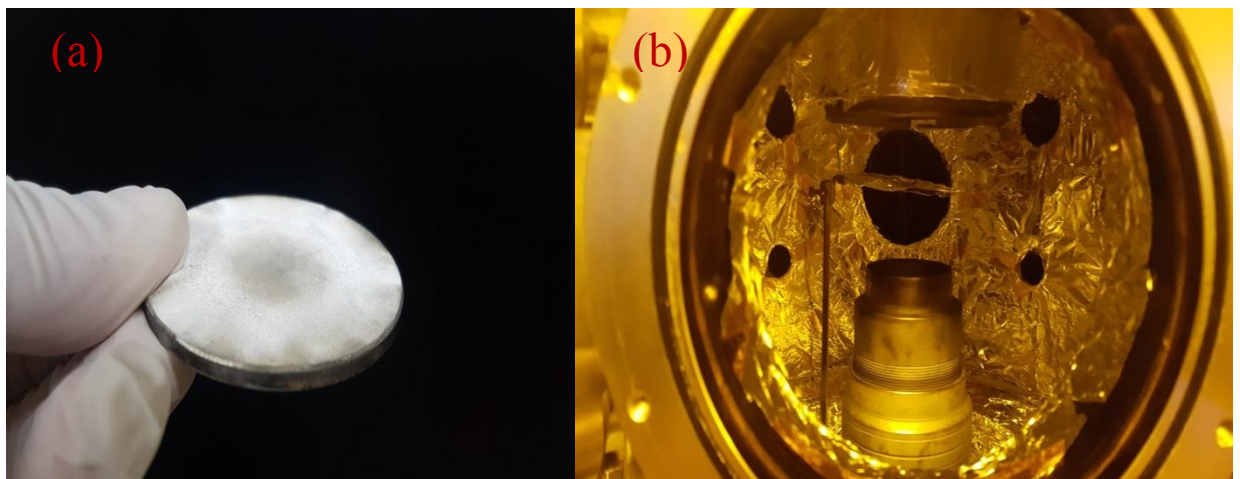
Fig. 3-2. (a) Optical image of Ag target, (b) Distance between the substrate and target in sputter chamber

After the sputtering chamber was evacuated with a pressure of 10 mTorr by using a rotary system, Ag nanoparticle was deposited at a deposition pressure of 8 mTorr at a gas flow ratio

14

of Ar:N_2 =1:10. The deposition rate was almost 1.7 nm/sec. An rf power of 130 W was used in the sputter chamber to create the plasma at a vacuum conditions of (∼8 K). The parameters are summarized in table 3-1

Table 3-1. Operating conditions for RF magnetron sputtering for Ag target

Target	Ag (99.999%)
Target-substance distance	7cm
Base pressure	10 mTorr
RF power	130 watt
Deposition pressure	8 mTorr
Deposition temperature	8 Kelvin
Deposition rate	1.7 nm/sec
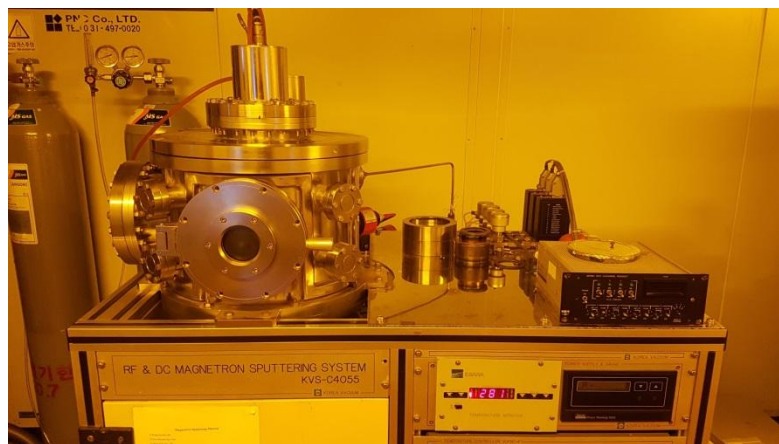
Fig. 3-3. (a) RF magnetron sputtering system

3.2. Ag nanoparticle optimization

To develop the Ag nanoislands and deploying an interfacial catalytic bimetal layer for

hydrogenation and dehydrogenation, it is highly desirable to optimize the Ag nanoparticles morphology which acts as a template for growing the nanoislands/bimetal structure. For optimizing the Ag morphology, a Keithely probe station system was used for checking the surface conductivity as it is believed that a highly agglomerated and bulk size nanoparticle may connected together tightly and increases the surface conductivity [38]. Furthermore, a bulk morphology with highly dense metal nanoparticle has a higher surface energy which could hinders the nanoislands grow as a higher surface energy will tend to reduce the surface diffusion process.
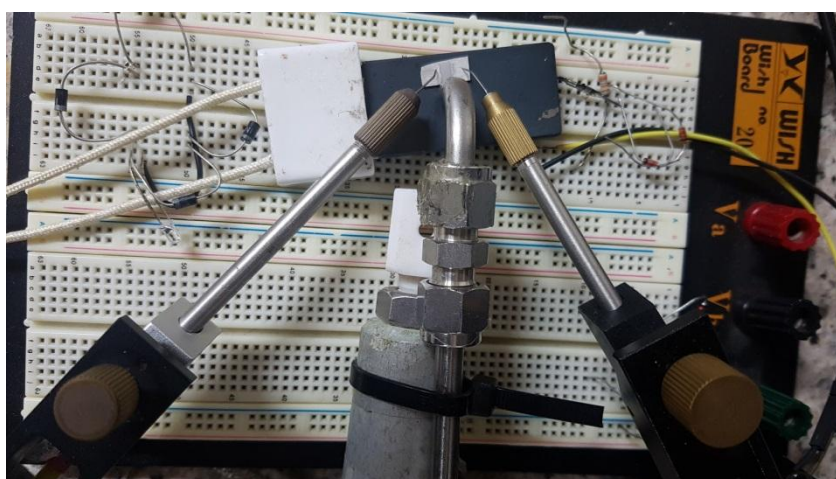
Fig. 3-3. Surface conductivity measurement

Hence, to optimize the Ag nanoparticle morphology, different sizes of nanoparticles were deposited by varying the deposition time in RF magnetron sputtering. The conditions and optimized size results are summarized in table 3-2.

Table. 3.2 Ag nanoparticle size optimization by RF magnetron system

Average nanoparticle size (nm)	Deposition time (Sec)	Surface resistivity (Ω)
10	~6	~30×10^6
18.50	~11	~10×10^4
34	~20	~3×10^3

After the deposition of Ag nanoparticles on alumina substrate, it's water contact angle was checked. A contact angle of 112.5° and 28.79 mN/m solid vapor interfacial energy was found for 18.50 nm sized Ag nanoparticles deposited on alumina substrate.

Fig. 3-4. Water contact angle of 18.50 nm Ag on alumina

This morphology provides an optimized surface conductivity of 10×10^4 Ω that was enough to induce an thermal annealing diffusion process due to the optimized surface energy between the nanoparticles and substrate. In table 3.3, the surface energy and water contact angle are summarized

Table 3.3 Water contact angle and surface energies of Ag nanoparticles

Average nanoparticle size (nm)	Contact angle	Surface energy γ_{SV} (mN/m)
10	105˚	14.34 mN/m
18.50	112.5˚	28.79 mN/m
34	125˚	35.56 mN/m

3.3. Ag nanoislands development

After depositing and optimizing the Ag nanoparticles on the alumina, a thermal annealing process was deployed to develop the Ag nanoislands. A vacuum pump was used to create a vacuum chamber. The annealing was performed at the presence of argon environment where a mass flow controller utilizes a 200 SCCM gas through a channel to the annealing chamber. A three stage annealing process was programmed. For the first or initial stage, the temperature remains around 5˚C and at a ramp of 20˚C/S it reach to 200˚C at the second stage where the time duration was programmed for 2 minute. Later, a step down process (third stage) at a slower ramp of 5˚C/sec were conducted. Several temperatures (300 ˚C, 350˚C, 400˚C, 450˚C, 500˚C, 600˚C) were applied for an equal time of 2 minutes to induce different islands morphology.

Fig. 3-5. Rapid thermal annealing system

After the rapid thermal annealing process, all the samples were cooled down at room temperature for a post sputtering process.

3.4. Bimetal deposition at Ag nanoislands

For enhancing the hydrogenation and dehydrogenation catalytic phenomenon, Pt/Pd bimetal was deposited at Ag nanoislands after the rapid thermal annealing process.

A Pd target of 99.999% purity was used and a distance of 7cm was maintained between the substrate and target in sputtering chamber. The depositing conditions are summarized in table 3.4.

Table. 3.4 Pd nanoparticle deposition conditions

Target	Pd (99.999%)
Target-substance distance	7cm
Base pressure	10 mTorr
RF power	160 watt
Deposition pressure	8 mTorr
Deposition temperature	8 Kelvin
Deposition rate	1nm /sec

Pt metal target of (99.999%) purity was deposited after Pd deposition by varying the RF magnetron sputtering system's operating conditions. The conditions are given in table 3.5.

Table 3.5 Pt nanoparticle deposition conditions

Target	Pt(99.999%)
Target-substance distance	7cm
Base pressure	10 mTorr
RF power	170 watt
Deposition pressure	8 mTorr
Deposition temperature	8 Kelvin
Deposition rate	1.42 nm /Sec
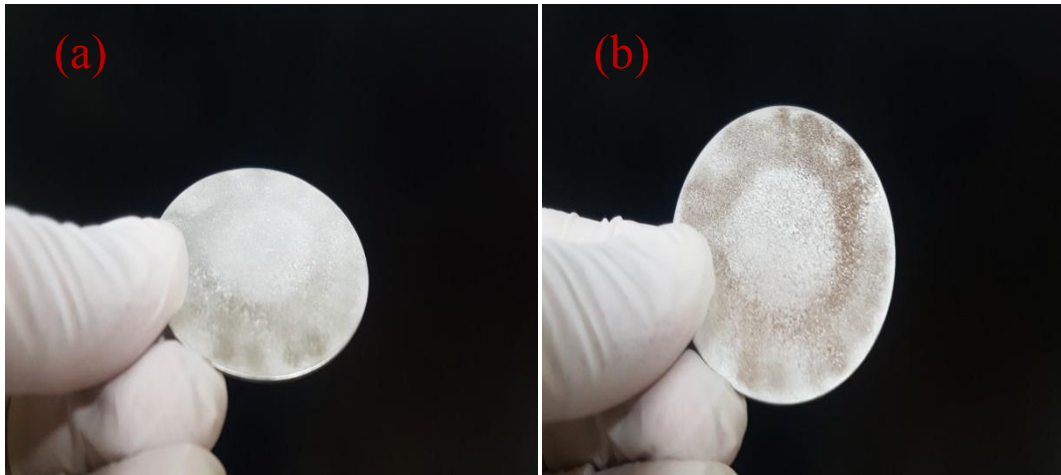
Fig. 3-6. Pd target, Pt target (a,b)

3.5. Electrodes deposition

After bimetal deposition, silver paste was used to put two electrodes at 2 mm apart from each other following a 50°C hot plate treatment for 3 hour. The optical image of as fabricated device has been shown in fig. 3-7.
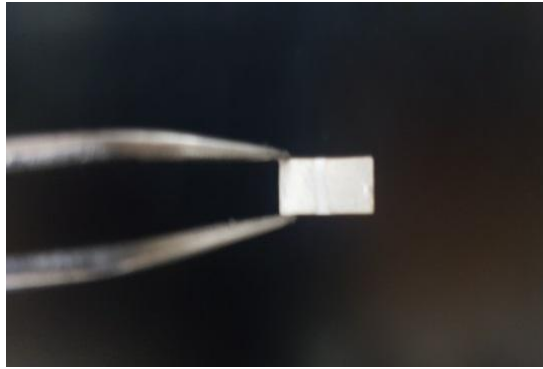
Fig.3-7. Optical image of as prepared device

3.6. Device fabrication process, in brief
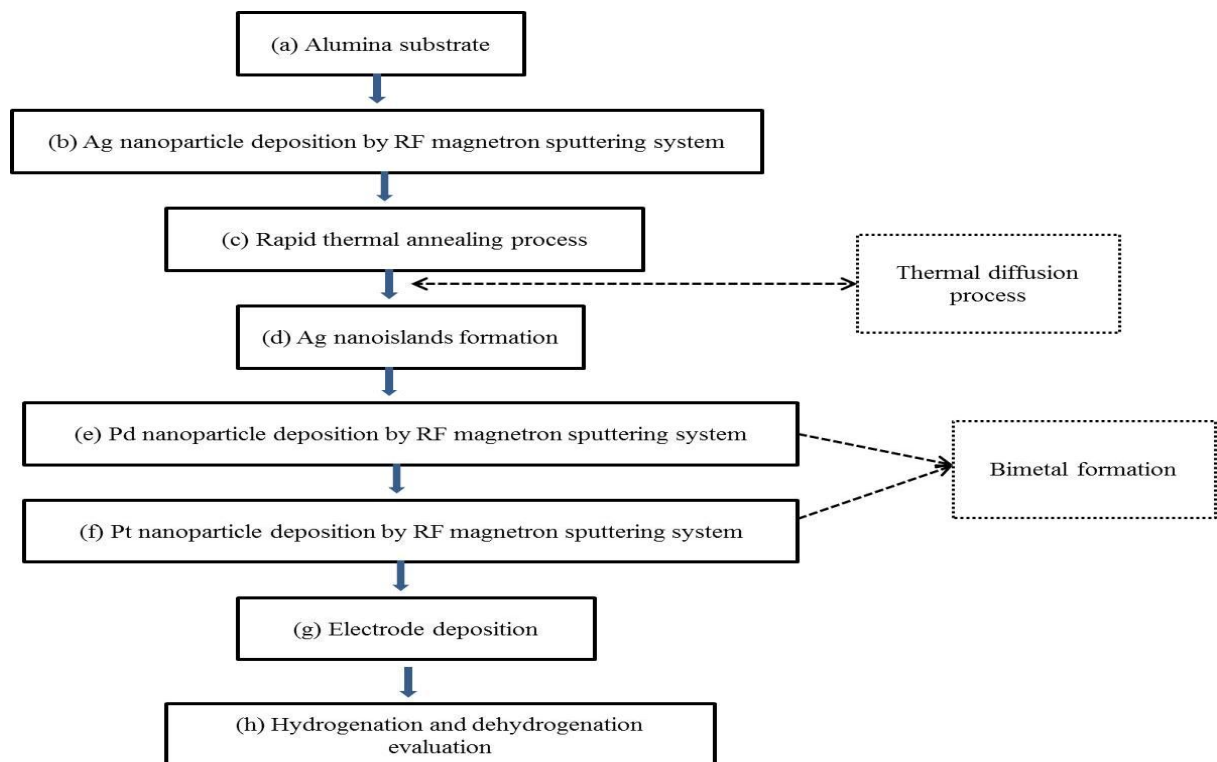
Fig. 3-8. Flow chart of device fabrication
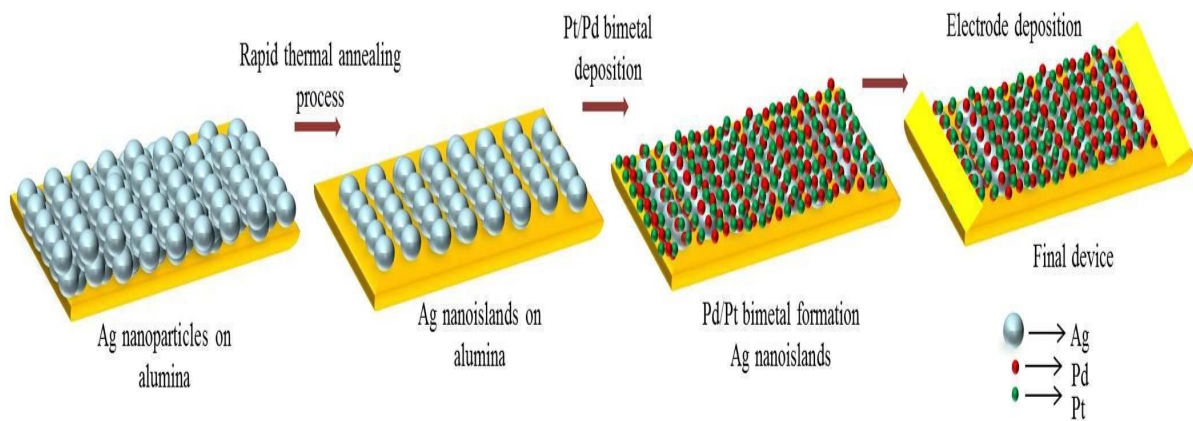
Fig. 3-9. Schematic image of device fabrication

3.7. Evaluation methods: Pt/Pd@Ag nanoislands decorated alumina substrate for fast hydrogenation and dehydrogenation

Figure 3.7 shows the schematic representation of the device fabrications steps.

Table 3-6. Evaluation methods

Morphology evaluation	For measuring electrical property and hydrogenation, dehydrogenation property
SEM, FESEM	Measuring hydrogenation and dehydrogenation response magnitude
Water contact angle	Temperature effects on response and recovery
AFM	Dynamic response (Hydrogenation and dehydrogenation at different gas concentrations)
EDS elemental analysis	Computational analysis in COMSOL Multiphysics for bimetal Size optimization
EDS mapping	
XRD	
XPS	
PL spectroscopy	

3.7.1. SEM (Scanning electron microscopy)

SEM is a highly rated microscopy tools by which high resolution images better than 1

nm can be achieved. A focused beam electrons scans the surface of the sample by interacting with the atoms of the sample and produces various signals that can be detected which provides information about sample's topography and composition. In this thesis, the surfaces of the nanostructured materials were characterized by using a JSM JEM – 7600F field emission scanning electron microscope (FE-SEM).

3.7.2 Water contact angle system

The hydrophobicity and surface energies of the nanomaterials were checked by Kruss DSA 100 drop shape analyzer using the sessile drop method at room temperature. Distilled deionized water droplets were dropped on the thin film surfaces using a micro-syringe.

3.7.3 Atomic force microscopy

AFM is a high-resolution scanning probe microscopy which can provide the nanomaterials image on the order of fractions of a nanometer, more than 1000 times better than the optical diffraction limit [58]. The morphology of the nanostructured Ag islands root mean square grain size was analyzed with (Multimode V, Vecco, USa) atomic force microscope (AFM).

3.7.4 EDS elemental analysis and mapping

Energy dispersive X-ray spectroscopy provides the elemental and compositional information of the nanomaterials along with chemical characterization. An interaction of the excited x-ray source and sample provide all the atomic and weight % of the nanomaterials. Furthermore, it also provides specific x-ray emission spectrum of each element. In this thesis, the atomic and weight % of each nanomaterial and their distribution was evaluated by EDS.

3.7.5 X-ray diffraction (XRD)

By using the x-ray diffraction techniques, the atomic and molecular structure of a crystal can be evaluated. The crystalline atoms causes the electron beams to diffract in different angle with different intensities that can produce a three dimensional picture of the atoms in the crystal. The crystalline properties of Pt/Pd@Ag nanoislands decorated alumina was analyzed with x-ray diffraction (XRD) (XRD, Rigaku Ultima IV) with Cu Kα ($\lambda = 0.154$ nm) radiation over a 2θ scanning range of 10-90˚).

3.7.7 X-ray photoelectron spectroscopy (XPS)

XPS is a highly surface sensitive measurement technique that evaluates the elemental composition, chemical state, electronic state, of the material at the parts per thousand range. It simultaneously measures the kinetic energy of a beam of x-rays and number of electrons that escape from the top 0 to 10 nm of the material. The electronic and chemical state of the bimetal interface with Ag nanoislands was analyzed by Al Kα radiation as the X-ray source.

3.7.8 Photoluminescence spectroscopy

Photoluminescence spectroscopy utilizes the emission of light from any form of matter after the absorption of photons. It is used to evaluate information about identification of surface, impurity levels, and interface. It's a very useful tool to check the metal oxide defects. The defects in Ag nanoislands after depositing bimetal were analyzed by PL spectroscopy.

3.7.9 Computational analysis

To evaluate the Pt/Pd size optimization was analyzed in COMSOL Multiphysics 5.1. An electric field distribution was checked on the bimetal interface after solving the boundary conditions for air and hydrogen medium.

3.7.10. Measuring gas sensing properties

The hydrogenation and dehydrogenation properties were checked in the kaithely probes station where a computerized mass flow controller (ATOVAC, GMC, 1200) system were used to change the concentration of H_2 gas in nitrogen (N_2) gas. The gas mixture was maintained at a constant flow of 50 sccm on the fabricated device which was mounted on an integrated heater.
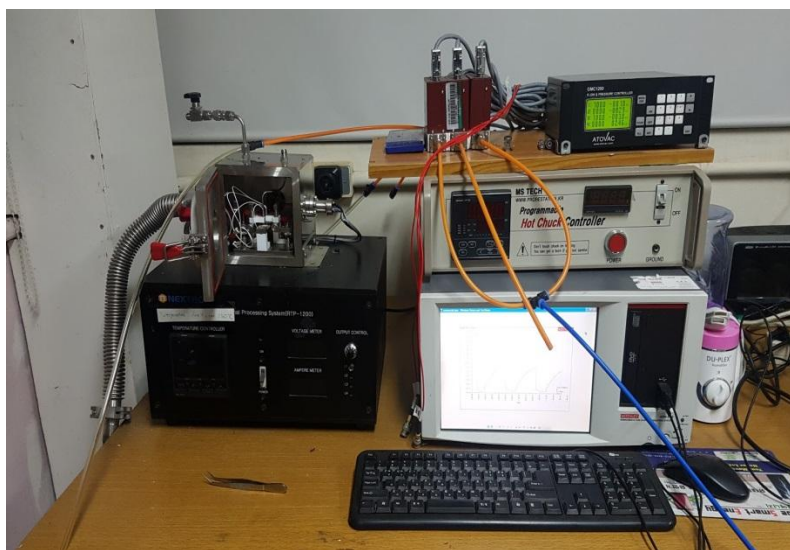
Fig 3.10. Hydrogenation and dehydrogenation measuring setup

3.8. Summary

In this chapter, the experimental steps and evaluations of Ag nanoislands based Pt/Pd bimetal on alumina was reported. The formation of the Ag nanoislands with detailed experimental procedures was illustrated. Detailed steps of the decoration of Pt/Pd bimetal @Ag nanoislands were also explained. Hydrogenation and dehydrogenation set up and gas measurement system was introduced. Characterization techniques for analyzing the nanomaterials morphology, crystal quality, metal oxides defects were listed with hydrogenation and dehydrogenation properties.

Chapter 4: Hydrogenation and dehydrogenation performance analysis of Pt/Pd@Ag nanoislands decorated over alumina

4.1. Materials structure and morphology:

In order to grow Ag nanoislands, two sizes of (18, 25 nm) Ag nanoparticles were deposited on alumina substrate by varying the condition in RF magnetron sputtering. Figure 4-1 (a), (b), shows the surface morphology of non-annealed Ag nanoparticles. Highly dense and agglomerated nanoparticles can be observed from the surface which represents an irregular formation of nanoparticles. A thicker nanoparticles deposition might not be enough to form a continuously film as atoms deposited from the vapor phase undergo a series of kinetic processes, including thermal accommodation onto the substrate, surface diffusion of the atoms on the surface, dimmer formation to initiate formation and growth [39]. More deposited atoms may help to grow small islands, contact with each other, and then merge into larger, but still compact islands [40,41]. Comprising nanoscale Ag crystalline grains, thicker and merged Ag nanoislands can show tight connection between the Ag crystalline grains. This compact bulk islands formation can increase the conductivity to very high label which need to be optimized for catalytic gas permeation process. However, some differences can be found in case of additional annealing process. A metastable configuration that tends to equilibrate through surface limited diffusion, once subjected to temperature by annealing [44].
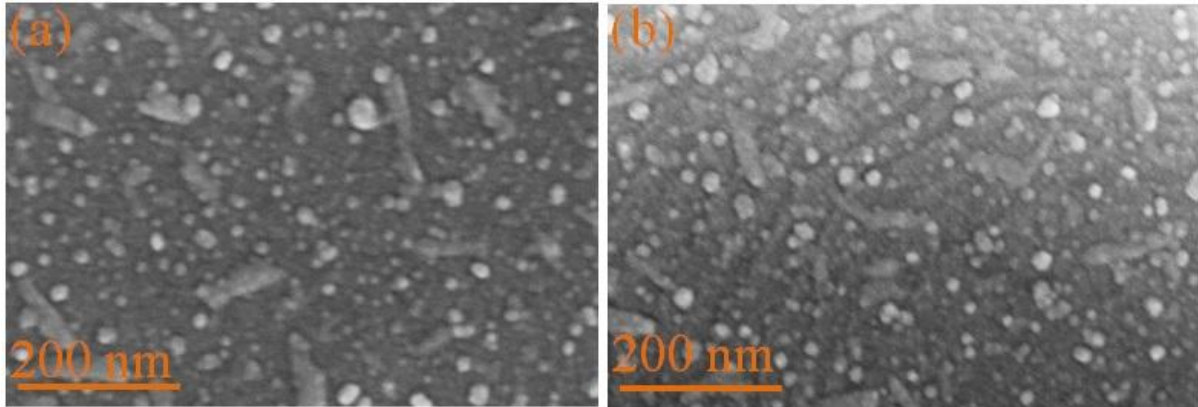
Fig. 4-1. surface morphology of Ag nanoparticles without annealing (a) 18.50 nm (b) 25 nm

The heterogeneous interfacial formation because of the differences in the surface energy between the rough alumina substrate and Ag nanoparticles can induce high fraction of grain boundaries, interfaces and surfaces, or residual stresses [45]. Thus, to maintain highly regular, small crystalline grains, nano sized metal islands structure, a post rapid thermal annealing process at some representative temperatures were performed with an initial film thickness of 18.50 nm. From the SEM observations in figure 4-2, it is obvious that the changes in the surface morphology of Ag nano islands accelerate with the increasing of the annealing temperature. Figure 4-1 (a,b) shows the Ag nanoparticles distribution without annealing whereas a less dense surface morphology can be observed from figure 4-2 (a) at 200°C annealing because of the connections between Ag domains separated after annealing process. A gradual diffusion away phenomenon was observed with increasing the temperature until 600˚C at figure 4-2 (a-g). The Ag atoms might be diffused away from the high curvature of the grain where the surface free energy is less and it continued until an equalized surface is reached [46].
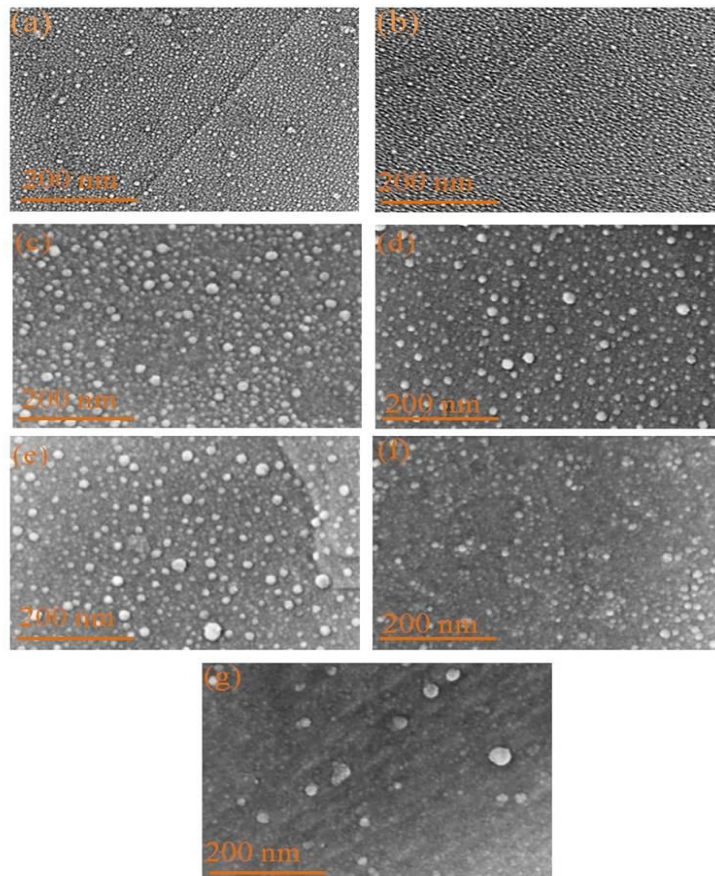
Figure 4-2. Surface morphology of Ag nanoparticles at (a) 200°C, (b) 300°C, (c) 350°C, (d) 400°C, (e) 500°C, (f) 550°C, (g) 600°C

By changing the average inter distances among the grains, a more regular nanoislands formation can be seen from the respective cross section SEM observation at figure 4-3 (a-e). When the annealing temperature is at 200°C, the nanoislands are not fully separated (fig.4-3,a) and a periodic island's structure is visible. The surface free energy between the islands is not minimized enough to fully separate the islands [47]. Figure 4-3d shows the morphology of nanoislands at 400°C where some nanoislands are getting fully separated whereas figure 4-3(e) at 500°C shows fully separated nanoislands formation. We noticed, that as the annealing temperature increased, the small particle are lessened and the distances between Ag

30

nanoislands decreases and at a temperature of 600°C almost all Ag nanopaticles diffuse away from the substrate (fig.4-2g). This phenomenon agrees with the surface limited diffusion [47]. This process can be attributed to the variation of surface diffusion coefficient with temperature [48].
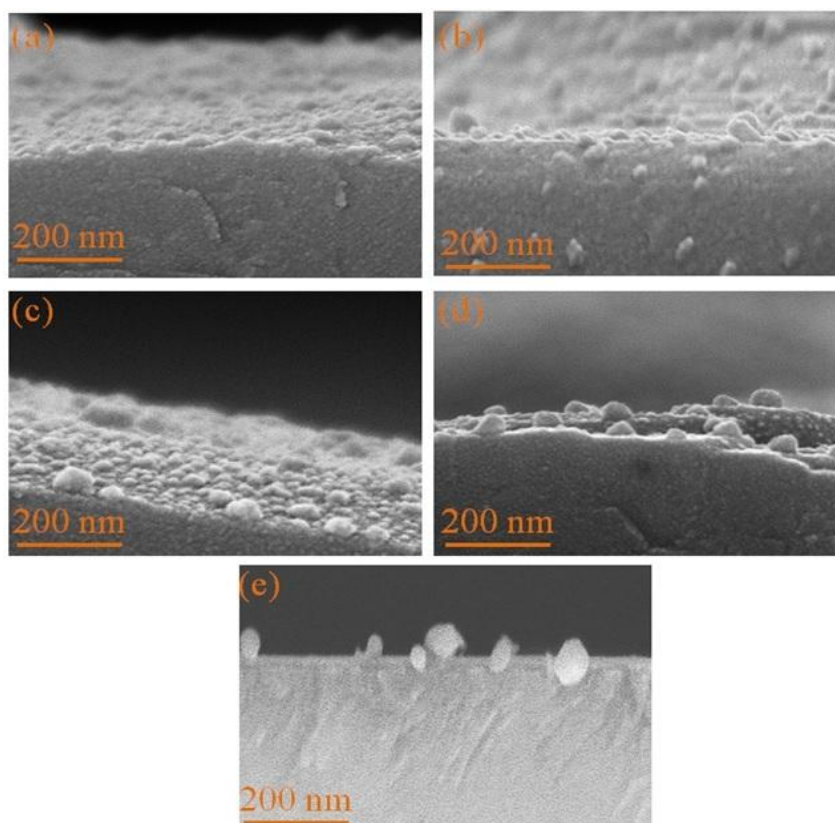
Fig. 4-3 Cross sectional view of Ag nanoislands at (a) 200°C, (b) 300°C, (c) 350°C, (d) 400°C, (e) 500°C

Due to the differences in the chemical potentials among the Ag nanoislands, the smaller nanoislands are thermodynamically unstable and they dissolve in atoms for each fixed temperature [49]. These smaller nanoislands get incorporated by other larger nanoislands in the rough alumina substrate [50]. This temperature incorporated surface diffusion process accelerates the probability of an arriving atom to find an existing island, rather than to form a

new island, resulting in the decrease in the silver particle density [51]. At a temperature of 600˚C, the Ag islands volatilize from the substrate and this phenomenon will be more obvious with the increase of the temperature [52]. It is also possible that, at higher temperature the rough substrate of alumina get acutely softer and it can't provide the stable interface for the diffusion of Ag atoms which can be seen from figure 4-2(g) [53]. Thus we conclude that 600˚C is high enough for the atom of our Ag nanoislands to volatilize from the rough alumina substrate, which leads to the absence of nanostructure on the substrate
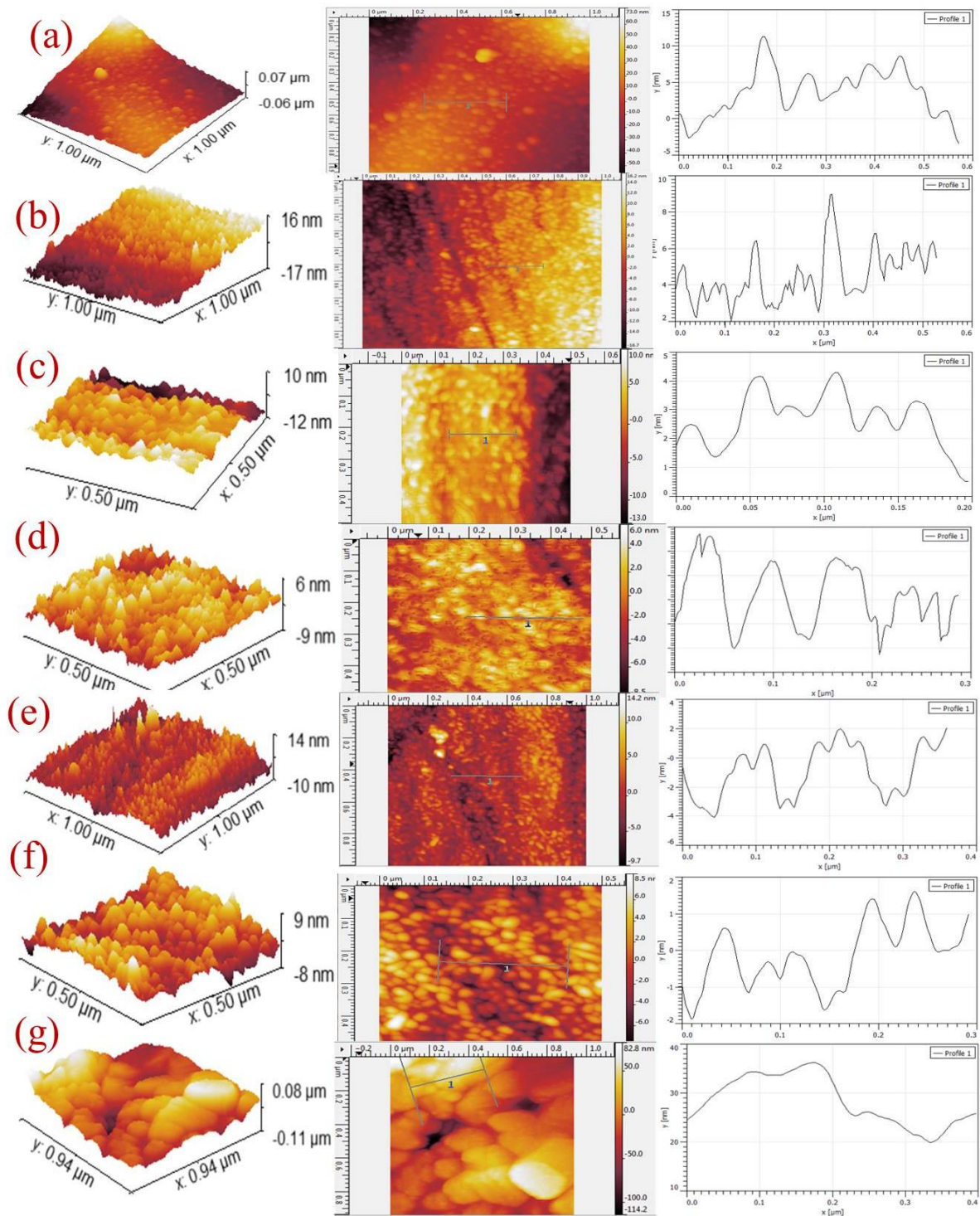
Figure 4-4(a-g) AFM analysis of Ag nanoislands (a) without annealing (b) 200℃, (c) 300℃, (d) 350℃, (e) 400℃, (f) 500℃, (g) 550℃

Figure 4-4(a-g) shows the variation of RMS grain size of Ag nanoislands annealed at different temperature (table 4-1). Before annealing, a RMS grain size of about 18.50 nm (fig.4-4a) was measured which later showed a gradual reduction with the increasing annealing temperature. However, at 600°C the RMS grain size shows a maximum value as all the Ag nanoislands volatize which was confirmed by SEM morphology (fig. 4-2g) leaving only the rough alumina substrate grains. Thus, from the AFM images, the decreasing trend of RMS grain size of Ag nanoislands (up to fig.4-4a-f) confirm the role of temperature dependent surface diffusion process. All the AFM measurement results are listed in table 4-1.

Table 4-1 RMS grain size of Ag nanoislands at different temperature

Sample	RMS grain size (nm)
Ag@alumina (non-annealed)	18.50
Ag@alumina at 200°C	6.5
Ag@alumina at 300°C	4.96
Ag@alumina at 350°C	2.63
Ag@alumina at 400°C	2.45
Ag@alumina at 500°C	1.76
Ag@alumina at 600°C	30
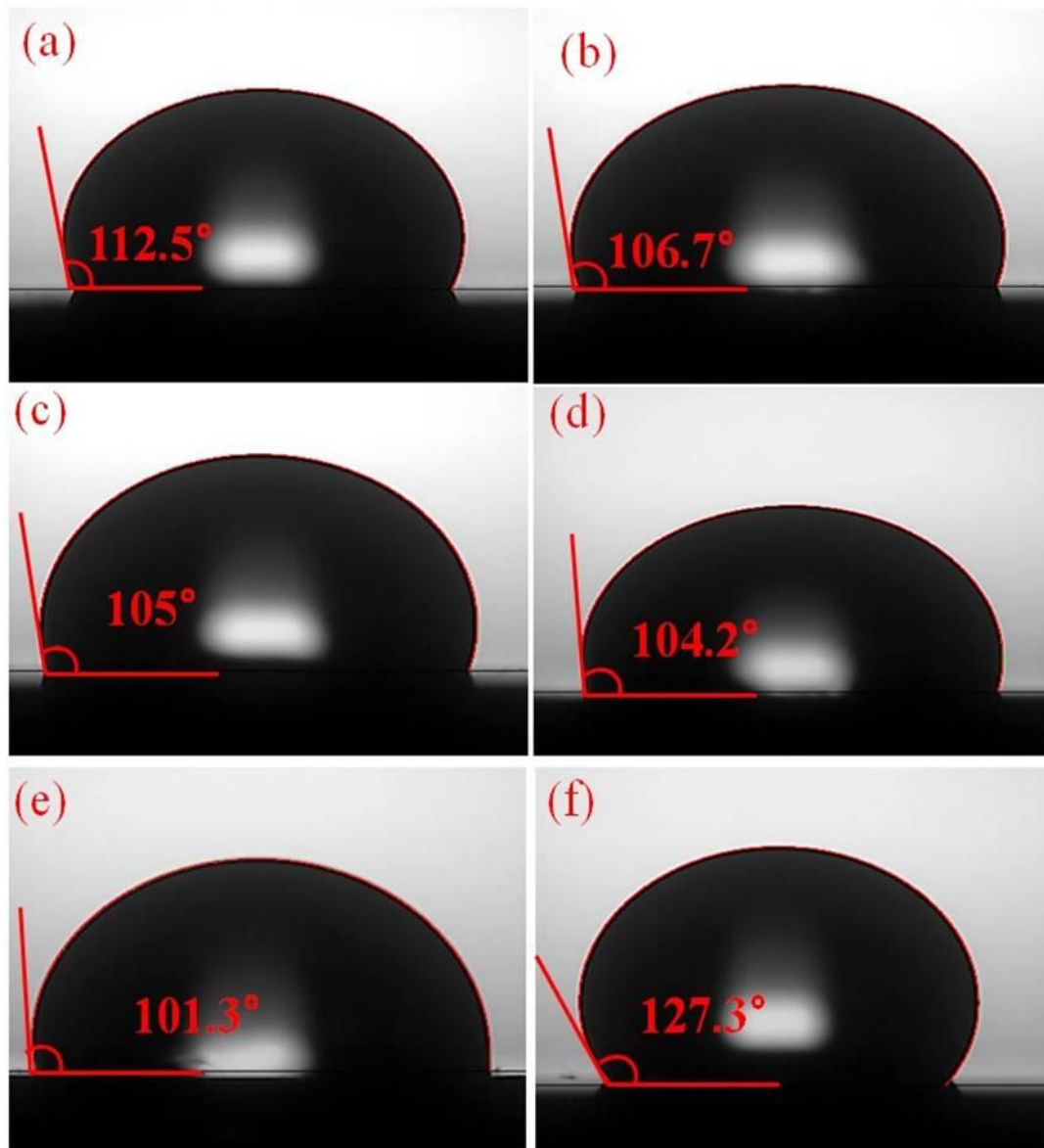
Figure 4-5 (a-f) Water contact angle of Ag nanoislands (a) without annealing, (b) 200℃, (c) 300℃, (d) 350℃, (e) 400℃, (f) Pt/Pd @ Ag nanoislands

To analyze the surface energy and hydrophobicity of the Ag nanoislands different morphologies, characterization with water droplets was carried out. The contact angle was measured according to Young's method [54], who first proposed a minimization model of three interfacial surface energies. The contact angle images of Ag nanoislands without

annealing (18.50 nm) (fig. 4-5a) and post annealed (fig. 4-5 b-f), Ag nanoislands with Pt/Pd bimetal was shown. The contact angle of non-annealed Ag nanoislands show a value of 112.5° which keeps decreasing with the increasing of annealing temperature. A lowest value of 101.3° was measured for an annealing of 400°C. It is well established that, if the contact angle is higher than 90°, the surface is hydrophobic, otherwise the surface is hydrophilic. Hence, all the samples show hydrophobic property and a maximum contact angle value of 127.3° was found after depositing 10/10 nm Pt/Pd bimetal for hydrogenation purpose. Thus, it can provide a stable performance in the H_2 gas as water molecules can't become stuck on the surface and decelerate the response. From the AFM measurements, it was observed that, RMS grain size keeps reducing with the annealing process which also can incorporate the gradual reduction of RMS roughness (table 4-1) and can also be analyzed from the hydrophobicity of the samples. It has been proven that, the RMS roughness or grain size is proportional with the hydrophobicity [55]. From the water contact angle measurements, we can see the gradual reduction of the hydrophobicity with the increasing of annealing temperature (fig. 4-5a-e). Additionally, the hydrophobicity is inversely proportional with the surface energy of the film surface. To determine the surface energy, the equation of Owens and Wendt and the Fowkes theory was used [56].

$$\gamma_{SV}^D = (\gamma_{lV}/4)\,(Cos\theta + 1)^2 \tag{4.1}$$

$$(\gamma_{SV}^D \gamma_{lV}^D)^{1/2} + (\gamma_{SV}^P \gamma_{lV}^p)^{1/2} = \gamma_{lV}(Cos\theta + 1)/2 \tag{4.2}$$

Where γ_{SV}^D, γ_{lV}^D, γ_{SV}^P, γ_{lV}^p, are the dispersive and polar components of solid-vapor (γ_{SV}) energy and liquid-vapor (γ_{lV}) energy, respectively. The surface energy calculated using this method for all the samples follows a similar fashion. The surface energy of each samples

calculate by the above method are listed in table 4-2.

Table 4-2 Contact angle and surface energy measurements

Sample	Contact angle	γ_{SV} (mN/m)	γ_{SV}^{D} (mN/m)	γ_{SV}^{P} (mN/m)
Ag@alumina (non-annealed)	112.5˚	28.79	28.11	0.68
Ag@alumina at 200˚C	106.7˚	28.72	28.575	0.14
Ag@alumina at 300˚C	105˚	29.88	29.72	0.16
Ag@alumina at 350˚C	104.2˚	31.78	31.44	0.34
Ag@alumina at 400˚C	101.3˚	32.816	32.58	0.236
Pt/Pd@200˚C annealed Ag nanoislands on alumina	127.3˚	24.210	22.128	2.08

The surface energy of the samples are gradually enhancing with the increasing of the annealing temperature as the contact angle slowly reduces. The interdistance among the nanoislands keeps increasing along with annealing temperature. Furthermore, the surface energy also keeps increasing with thermal annealing that reduces the contact angle of the Ag islands. This confirms the surface diffusion process which is induced by thermal diffusion coefficient annealing. It also confirms the AFM measurements as the RMS grain size shows a reduction trend with increasing of annealing temperature.

Thus, to utilize the minimum distance between the Ag nanoislands at 200˚C, we deposited

nano sized hydrogen sensing Pt/Pd bimetal which makes a percolated pathway by hydrogen induced lattice expansion and columb scattering upon hydrogenation [56]. To confirm the Pt, Pd crystal size and their bimetal formation on Ag nanoislands (annealed at 200˚C), we conducted high resolution XRD analysis. Figure 4-6 shows the XRD pattern of the Pt/Pd@Ag nanoislands for pre and post annealing case.
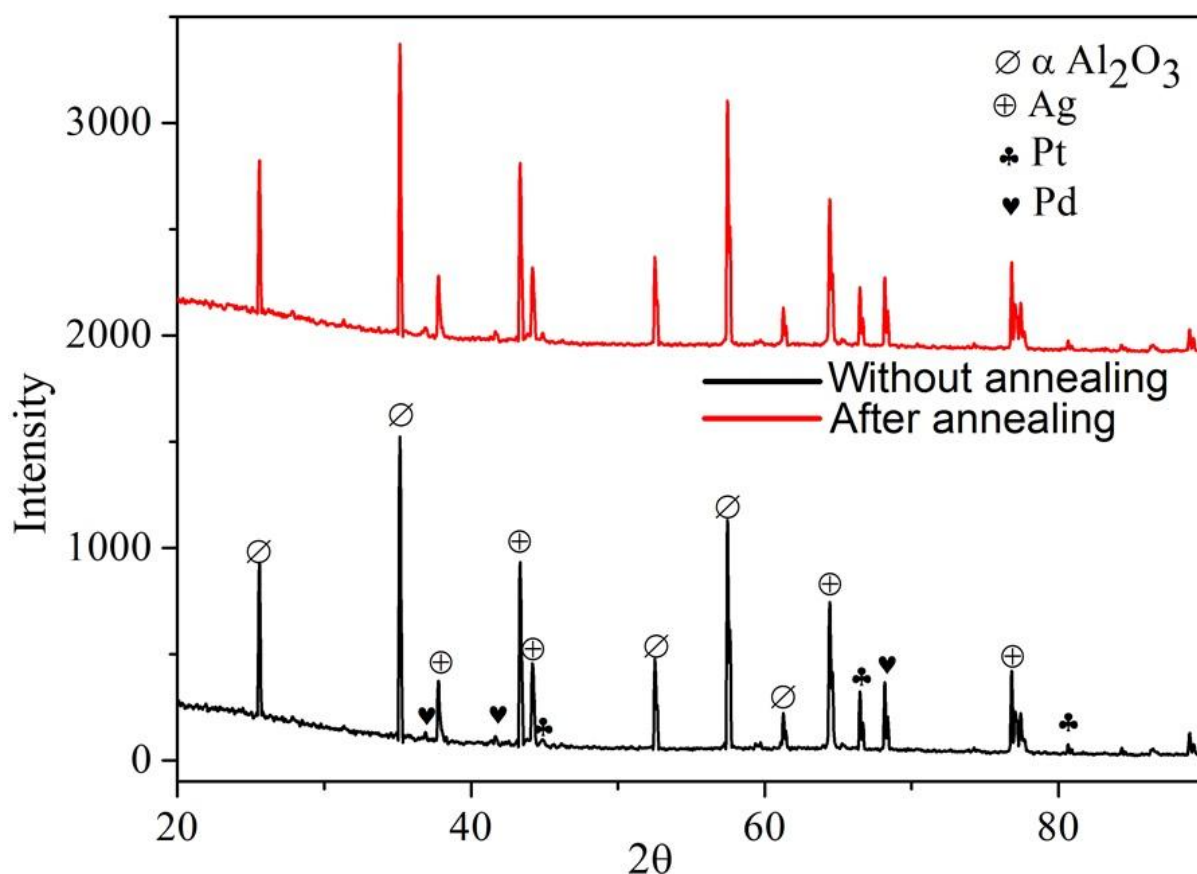
Figure 4-6. XRD analysis

The most intense diffraction peak at $2\theta = 34.94°$ can be indexed to the (104) plane of α-Al_2O_3 [57]. In addition, the diffraction peaks observed at 2θ values of 38.26˚, 44.44˚, 64.66˚ are corresponding to the monometallic Ag (111), (200), (220) planes of fcc crystalline structure and peak at $2\theta=68.23°$ corresponds to monometallic Pd (220) planes of fcc

crystalline structure [57-60]. A small peak originating at 2θ=42.5˚ can be indexed to Pd/Ag interfacial alloy formation as it remains between the monometallic ag peaks of 2θ=38.26˚ and 44.44˚ while the monometallic Pd peak of 2θ= 40.15˚ (111) might be proceeded towards higher 2θ values because of lattice mismatch formed by Ag/Pd interface [60, 61]. The intermetallic Pd/Ag peak at 2θ=42.5˚ broadened by a smaller amount for the annealed Ag nanoislands at 200˚C concludes that the size reduction of Ag nanoparticles. Peaks at 2θ=46.3˚, 67.56˚ are corresponding to the (200) and (220) of platinum for fcc crystal structure [61,62] and the diffraction peaks between the 2θ=42.5˚ to 46.3˚ may be originated from the complex interfacial formation of Pt/Pd bimetal with Ag nanoislands. The crystallite size for Ag, Pd, Pt, was calculated by using Scherer's formula and was found around 18.50, 10, 10 nm for each case respectively.

$$ß = Kλ/Dcosθ \tag{4.3}$$

Where ß is the crystallite size, λ is wave energy of X-ray source, D is the full width at half maximum and cosθ is the diffraction angle. The formations of Pt/Pd bimetal on nanostructured Ag nanoislands create a maximum hydrophobicity of 127.3˚ (fig.4-5f) with a lowest surface energy of 24.210 mN/m (table 4-2). This lowest surface energy also leads to smaller grains and reduced inter-grain distances [63]. Additionally, upon the deposition of the Pt/Pd bimetal @ Ag nanoislands on alumina, Pt capped the Pd and Ag nanoislands to form discrete bimetallic nanoparticles with high uniformity and nearly equal distances between grains. The uniform discrete manner may be formed by the lower surface energy and low polar components of the surface energy. It is well understood from the surface energy calculation (table 4-2) that reduced polar components are generally more hydrophobic.

Therefore, the sputtered atoms of metal attached with the surface with higher contact angle due to higher hydrophobic nature and maintain the uniformity towards the substrate [62, 63]. The EDS elemental composition of the as deposited Pt/Pd bimetal at different annealed Ag nanoislands on alumina (fig. 4-7) and an elemental mapping (surface and cross section fig.4-8, 4-9) was shown. The presence of aluminum (Al), oxygen (O), silver (Ag), Palladium (Pd), Platinum (Pt) and the absence of peaks related to contamination concludes the formation of high-purity surface for hydrogen gas sensing. A reducing trend of Ag atomic and weight % was observed for different annealed condition as the Ag nanostructure morphology changes.
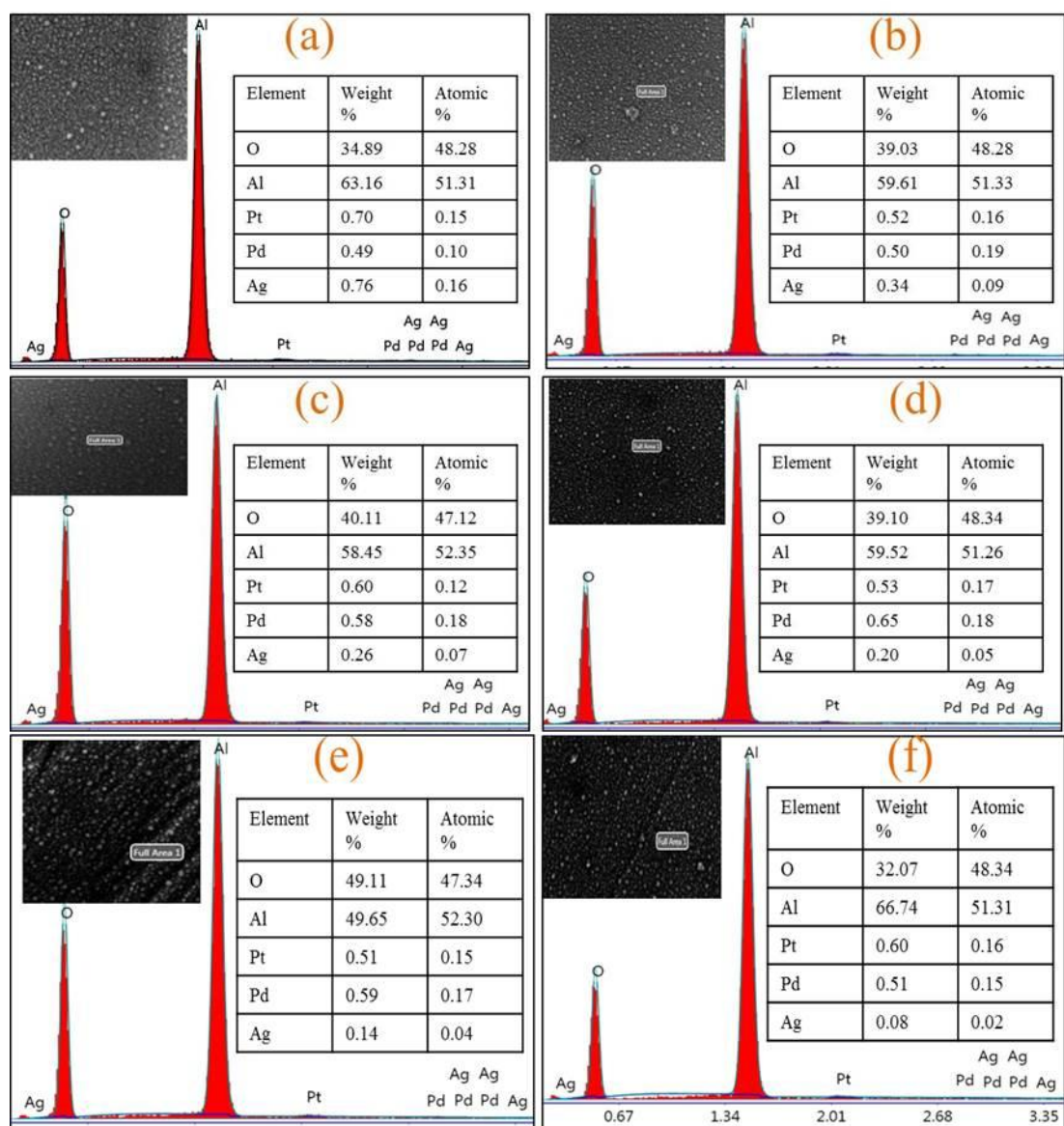
Figure 4-7 EDS elemental analysis of Pt/Pd@Ag nanoislands over alumina (a) without annealing (b) 200°C, (c) 300°C, (d) 350°C, (e) 400°C, (f) 500°C

A surface and cross sectional elemental mapping for the sample (Pt/Pd@Ag nanoisland on alumina at 200°C was shown in figure 4-8, 4-9 for observing the nanoparticles uniform distribution over the entire substrate. From the surface and cross sectional EDS mapping, it can be observed that Pt/Pd and Ag are distributed homogeneously over the substrate which further confirms the formation of a highly uniform Pt/Pd bimetallic thin film on Ag

nanoislands.
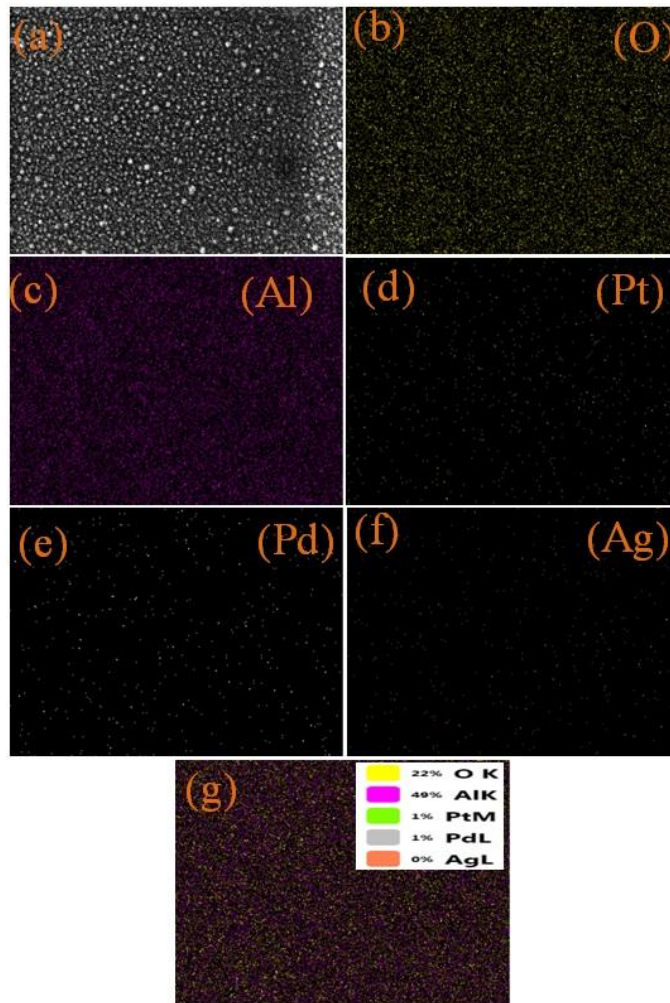
Figure 4-8. EDS mapping (surface) of Pt/Pd@Ag nanoislands over alumina substrate

Figure 4.10 shows the XPS analysis for examining the surface compositions of the Pt/Pd bimetal with the Ag nanoislnads at different annealing conditions. The morphological differences among the nanostructured Ag islands for surface diffusion coefficient at different temperature causes the interfacial composition to change for metal alloys.
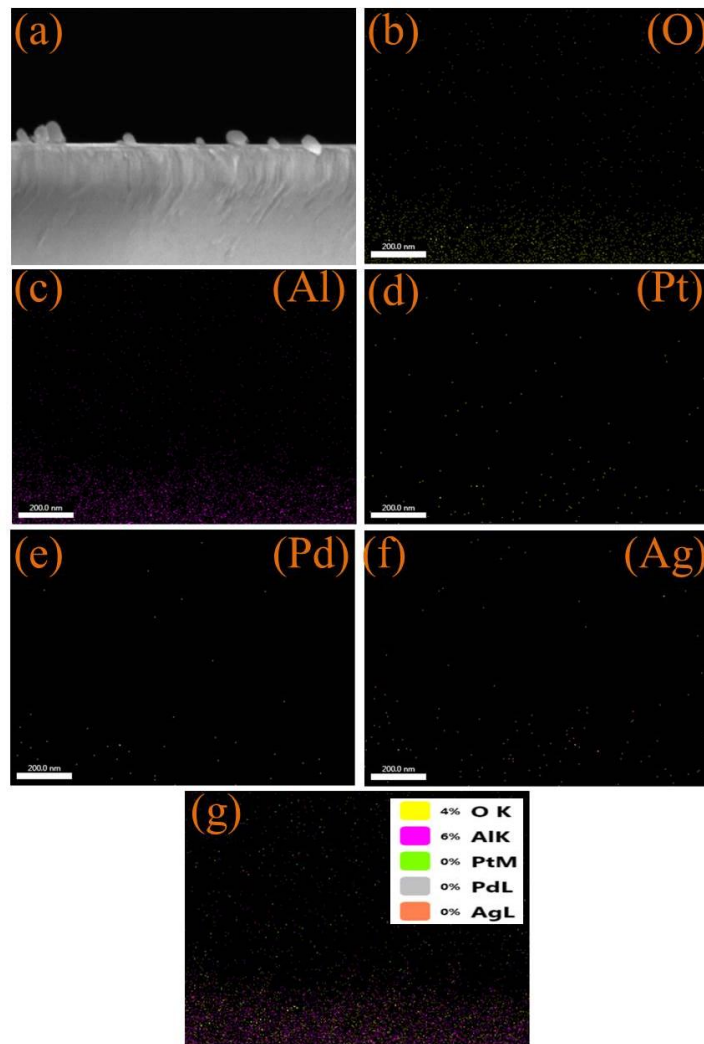
Figure 4-9. EDS mapping (cross sectional) of Pt/Pd @Ag nanoislands over alumina

The corresponding doublets of Ag 3d, Pd 3d, Pt 4f core levels were deconvoluted into Ag 3d $_{5/2}$, Ag 3d $_{3/2}$, Pd 3d $_{3/2}$, Pd 3d $_{5/2}$, Pt 4f $_{5/2}$, Pt 4f $_{7/2}$ by Gaussian- Lorentzain fitting method after linear background subtraction. A maximum shift in higher binding energies for Ag 3d $_{5/2}$ = 368 eV, Ag 3d $_{3/2}$ = 374 eV Pd 3d $_{3/2}$ = 340.5 eV, Pd 3d $_{5/2}$ = 335, Pt 4f $_{5/2}$ = 70.5, Pt 4f $_{7/2}$ = 74 for the sample Pt/Pd@Ag nanoislands for 200˚C was observed (fig.4-10b).
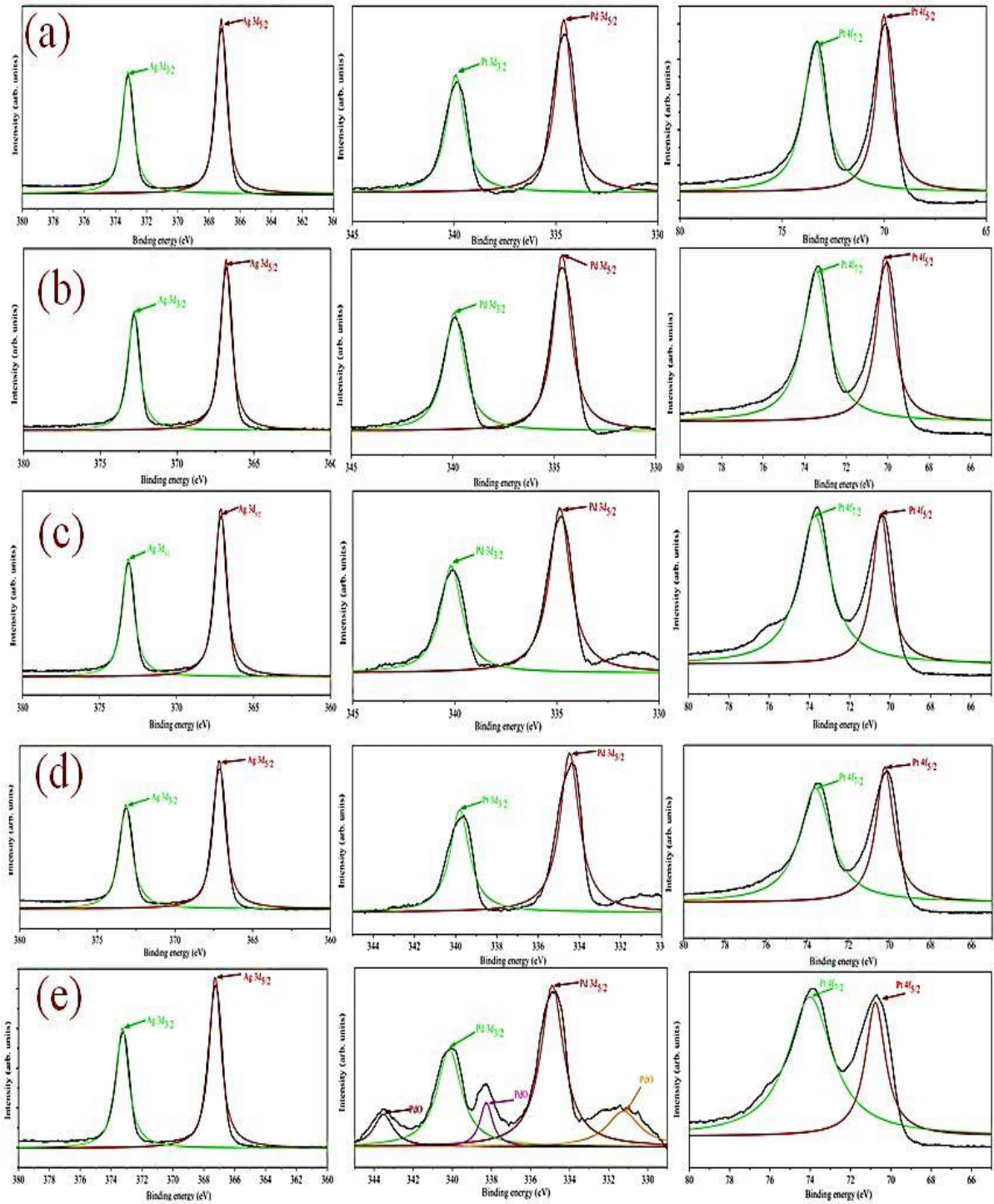
Figure 4-10. XPS analysis of Pt/Pd @ Ag nanoislands Surface morphology at (a) 200℃, (b) 300℃, (c) 350℃, (d) 400℃, (e) 500℃

These slight shifts can be promoted from the electronic interaction and maximum

interfacial alloy formation between the Pt/Pd bimetal and Ag nanoislands due to the differences in electron negativity [63, 64]. From the XPS measurements (table 4-3) It confirms that the bimetal alloys are tightly connected with the Ag nanoislands as the temperature diffusion induced separations are smaller for 200°C and 300°C cases which induce additional lattice strain or the higher number of electron donation from the bimetal [64,65]. All the measurements are summarized in table 4-3. Thus, a percolated pathway is constructed within the Ag nanoislands and remains strongly connected which can improve the surface conductivity.

Table 4-3. XPS measurements

Sample	Ag 3d$_{3/2}$ (eV)	Ag 3d$_{5/2}$ (eV)	Pd 3d$_{3/2}$ (eV)	Pd 3d$_{5/2}$ (eV)	Pt 4f$_{5/2}$ (eV)	Pt 4f$_{7/2}$ (eV)
Pt/Pd@ non-annealed Ag nanoislands on alumina	373.5	367.5	340	334.5	70	73.5
Pt/Pd@200°C annealed Ag nanoislands on alumina	374	368	340.5	335	70.5	74
Pt/Pd@300°C annealed Ag nanoislands on alumina	373.8	367.7	340.5	334.8	70.2	73.7
Pt/Pd@350°C annealed Ag nanoislands on alumina	373.5	367.3	340	335	70	73.8
Pt/Pd@400°C annealed Ag nanoislands on alumina	373	367.4	340	335	70	74

Figure 4-11 illustrates the photolumiscence of Pt/Pd bimetal distribution on the annealed (200˚) and non-annealed Ag nanoislands. A higher intensity of the photoluminescence was observed from the non-annealed Pt/Pd@Ag nanoislands as the larger amount of Ag (18.50 nm) is covered with oxygen which increases the defect states [46, 47, 48].
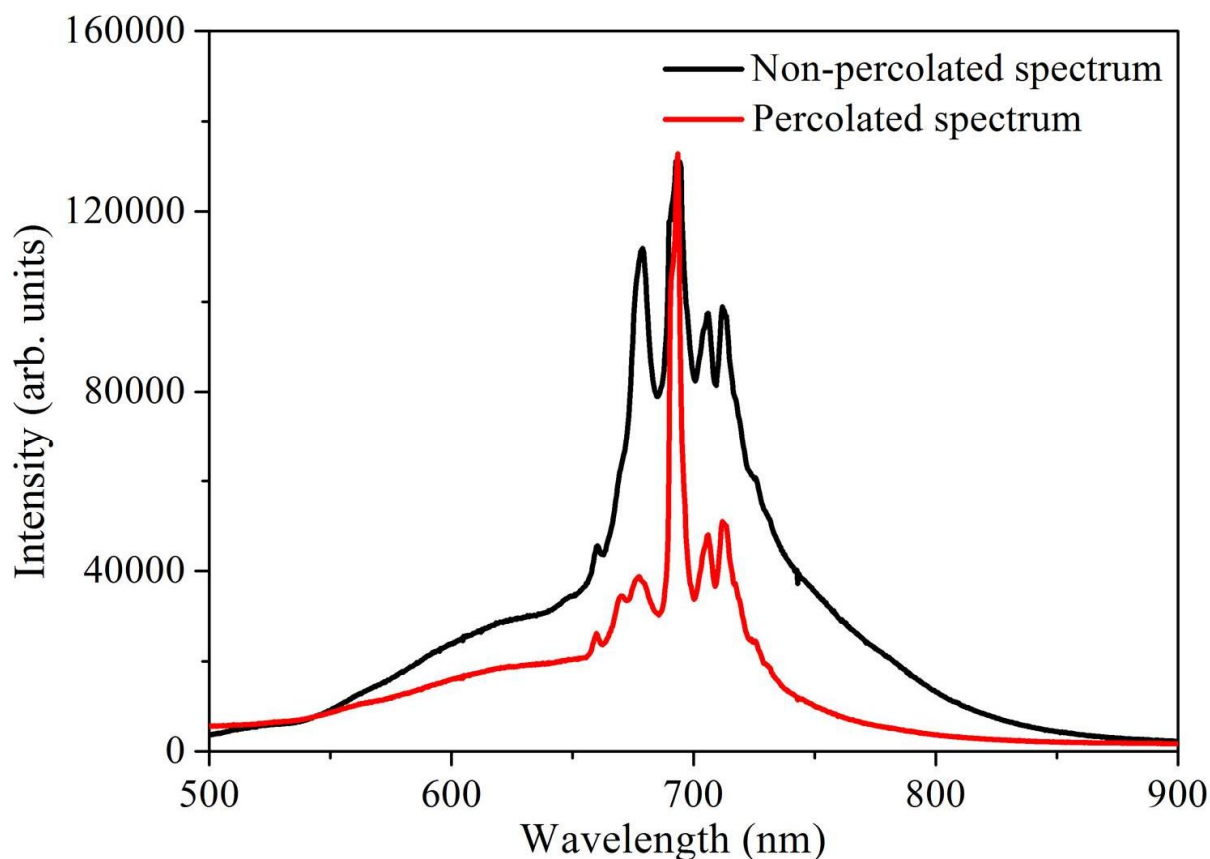
Figure 4-11. Photoluminescence spectroscopy

It can be possible that, because of the higher amount of silver atoms (fig 4-7a) and larger nanoislands with smaller distance; Pt/Pd bimetal can't fully cover the nanoislands surface. Thus, non-percolated surface is formed which shows higher oxidized defect states in photoluminescence. Whereas, in the post annealed sample, the intermixing alloy formation among the metals is good (fig 4-10b) show a less intense photolumiscence due to the uniform capping of Pt/Pd bimetal. A quantum confinement effect (QCE) is a possible mechanism

where the Ag nanoislands (6.50 nm) with Pt/Pd bimetal show less oxidized defect states that further confirms the tight connection and good capping of Pt/Pd bimetal over the Ag nanoislands [69, 70, 71, 72]. In this case, a highly percolated pathway can be formed that can increase the synergetic effects of the metal alloys [73].

4.2. Hydrogenation and dehydrogenation studies:

In the synthetic air environment, Hydrogen molecules physisorbs on the Pd surface and gradually dissociates into hydrogen atoms, chemisorbs in the Pd lattice structure for forming the Pd-hydride (Pd-H) as follows,

$$H_2 \text{ (g)} \longrightarrow 2H \text{ (ads)} \tag{4.4}$$

$$Pd + H \text{ (ads)} \longrightarrow Pd\text{-}H \tag{4.5}$$

Thus the dissociated Hydrogen atoms transform the metal to metal hydride phase by expanding the volume of Pd lattice structure which narrows the gaps between the neighboring clusters of nanoparticles [74, 75]. The electrical resistivity of Pd-H is almost a factor of 2 higher than that of pure Pd metal which allows detecting the hydrogen gas due to the increasing in the resistance value [76]. However, in an air environment, the presence of oxygen enables the formation of catalytic water molecules at the Pd surface that impedes surface coverage for chemisorbed hydrogen available to be absorbed [77,78]. This phenomenon decreases the Pd adsorption sites, lowering the hydrogen physical absorption [79]. Thus, it also extends the time required for Pd lattice structure to host hydrogen molecules at α-phase and transforming to Pd-H at ß-phase which eventually slows down the whole hydrogenation process [80]. Alloying the Pd lattice with Pt could change the surface chemistry as a favorable means in the aforementioned situation [81]. It was also reported that

Pt is a better catalyst for the hydride formation which is the rate limiting reaction for hydrogenation response for an optimum thermal condition (≥100˚C) [82,83]. Thus, optimizing the temperature and alloying with Pt can be an effective way to accelerate the hydrogenation performance of Pd thin film [84]. However, along with optimizing temperature, catalytic high surface area based Ag nanoislands can enhance Pt/Pd bimetal's synergetic effect. Highly regular Ag nanoislands formation (Fig.4-3b) on rough alumina substrate increases the surface to volume ratio which accelerates the interfacial alloy formation with the catalytic bimetal (Fig. 4-10b). In addition, the complex alloy formation may increase the response of hydrogenation permeation by increasing the active surface coverage. Furthermore, it was found that Ag alloying with Pd can be advantageous for the embrittlement and mechanical issue of Pd lattice which might be more improved with the Pt/Pd@ Ag nanoislands case [85, 86]. A higher surface to volume ratio based Ag nanoislands enhances the bimetal capping configuration that makes a percolation pathway that is suitable for higher carrier mobility [67, 88]. It is believed that, a hydrogen induced lattice expansion in nano sized catalytic sputtered bimetal may form a shorter conduction pathway for carrier mobility in the transduction process between physisorption to chemisorption on an insular substrate [89, 90]. However, maintaining the homogeneous nano sized bimetal capping structures are highly challenging and catalytic metal nanoislands structure beneath the bimetal structure increases the connection between the metal atoms and enhances the surface conductivity which may enhance the hydrogen induced lattice expansion faster. The induced hydrogen may scatter all the carrier charges by a coulomb scattering process which involves a charge variation in the catalytic metal alloys [86, 89, 91]. The schematic of the formation of percolated bimetal based on Ag nanoislands (Pt/Pd@Ag NI) and its hydrogenation process

are showed in Fig. 4-12.
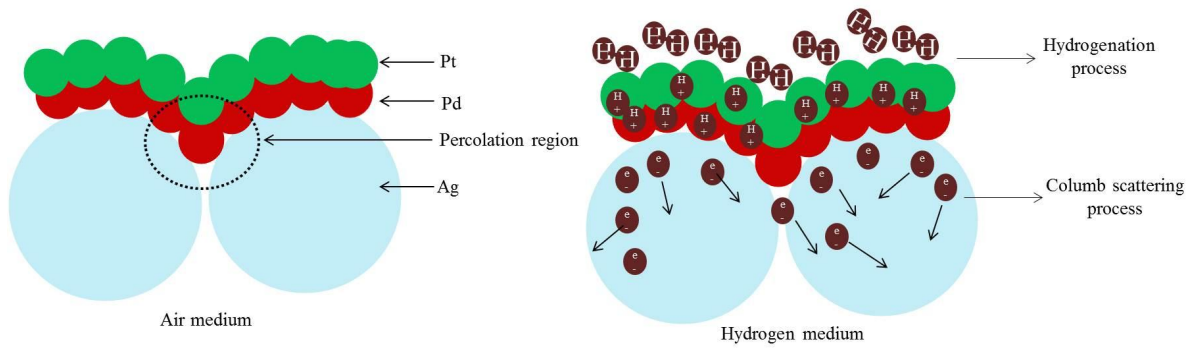
Fig. 4-12 Percolated pathway formation and hydrogenation mechanism (from left to right)

In Figure 4-13 (a-e), we observed a close relation between the base resistance and Ag nanoislands diffusion process, where a range of kΩ to GΩ was measured depending on the separation distance between the islands (Fig. 4-3).
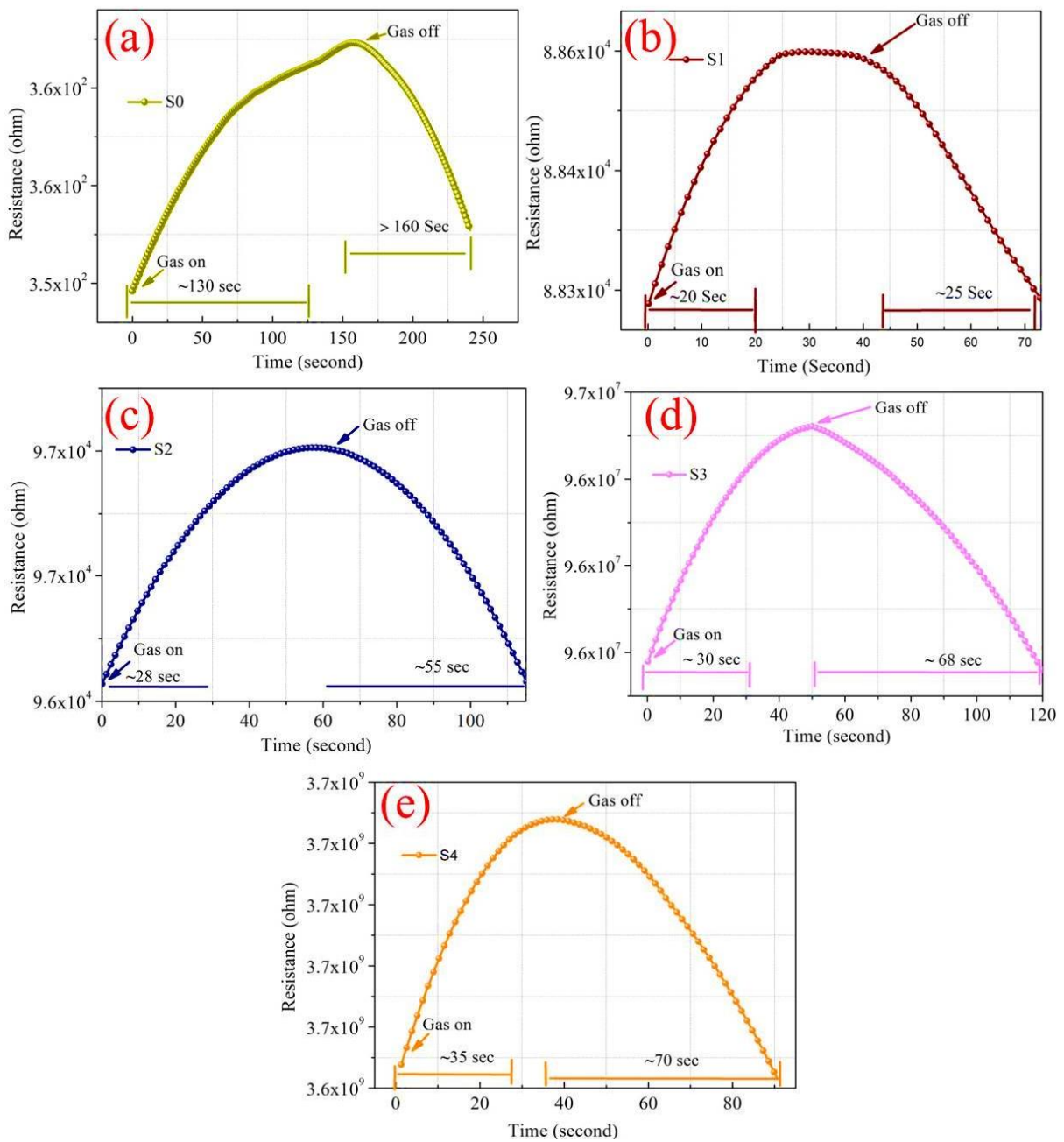
Figure 4-13. Response and recovery time of (a) Pt/Pd @ non-annealed Ag nanoislands (b) Pt/Pd @ 200°C annealed Ag nanoislands (c) Pt/Pd @ 300°C annealed Ag nanoislands. (d) Pt/Pd @ 350°C annealed Ag nanoislands (e) Pt/Pd @ 400°C annealed Ag nanoislands

An optimized conductivity is also necessary for the catalytic alloy formation and the surface

energy. Apart from the nanoislands separation, we also analyzed Pt/Pd bimetal thickness effect and their charge density. A computational analysis was done in COMSOL Multiphysics to optimize the Pt/Pd size and their charge density in the interfacial alloy (fig. 4-14).
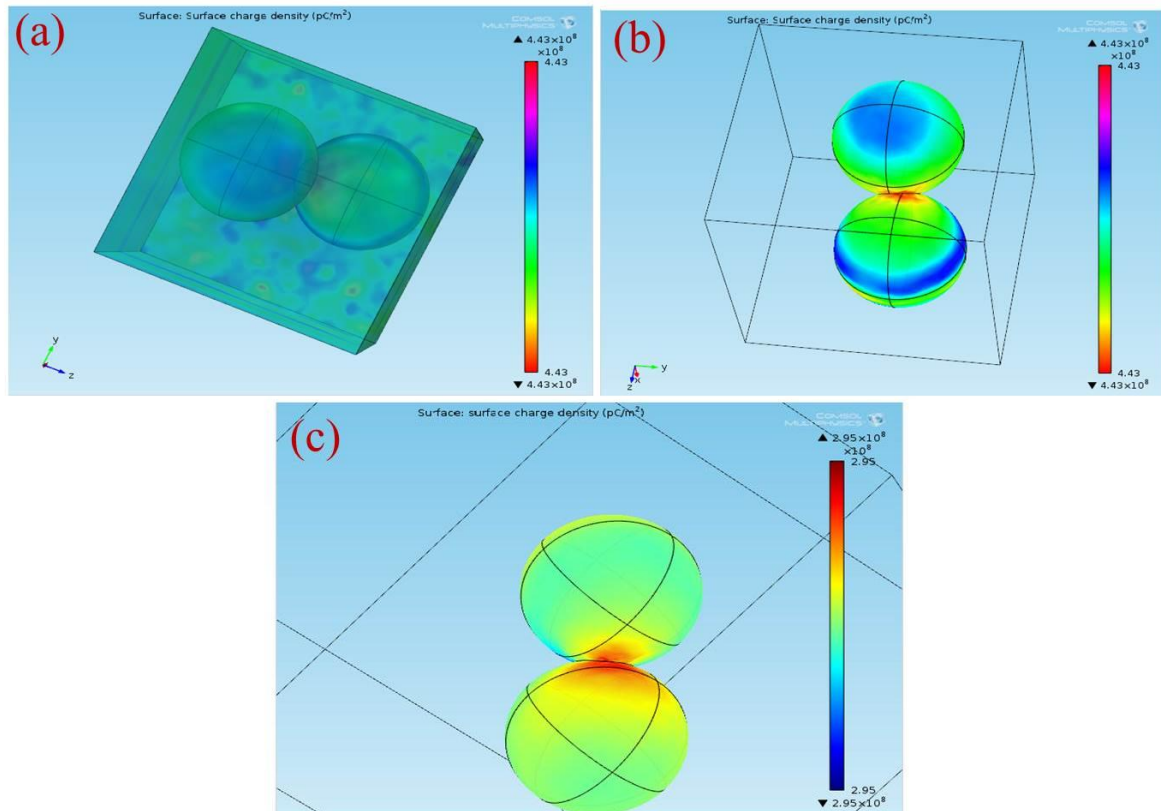
Figure 4-14. Computational analysis of Pt/Pd (5/5 nm) bimetal (a) Surface charge density at the interface of bimetal (b) at air environment (c) at hydrogen environment
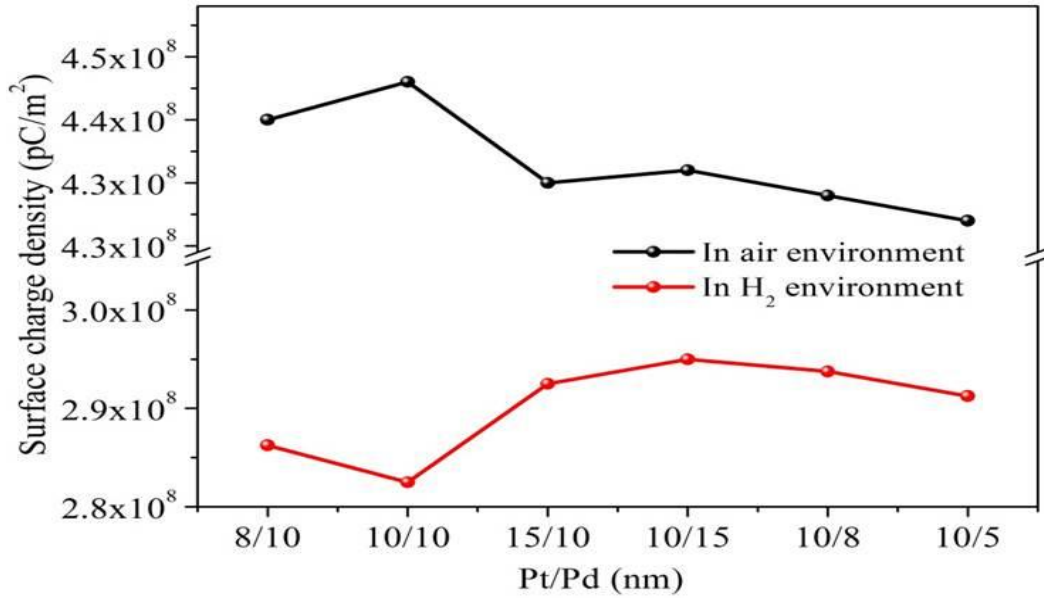
Figure 4-15. Simulation results of Pt/Pd bimetal

The simulation was performed up to 15 nm for Pt and 10 nm for Pd , as a thicker Pt layer can form a barricade to the injection of the hydrogen molecules to the Pd surface; which may impedes the sufficient hydride formation for Pd; furthermore, the hydrogen induced expansion of Pd might be hindered due to the excessive strain imposed the Pt capping layer, and the catalytic water formation at the Pt surface can be enhanced, hence slowing down the hydrogenation response [63, 87]. Figure 4-14(a-c) illustrates the distribution of electrical permittivity of the Pt/Pd bimetal (10/10 nm), which reveals that a certain applied potential difference on the boundaries of the chamber creates a surface charge density depending on the medium (air, hydrogen) in the chamber inside. A highly dense surface charge density (Fig. 4-14a, b) can be observed from the interface of Pt/Pd bimetal as the relative permittivity of Pt/Pd bimetal is much higher ($\varepsilon_r = 67.88$) in comparison to bare Pt ($\varepsilon_r = 17.19$) and Pd ($\varepsilon_r = 13.69$) [88]. We found a maximum amount of surface charge density (table 4) for Pt/Pd (10/10 nm) case in air environment and a lowest value in hydrogen environment from all other thickness variation. This result concludes that, a maximum amount of

hydrogen physisorption and chemisorption might occur in case of uniform 10/10 nm Pt/Pd bimetal case, hence effectively increases the electrical resistance of the bimetal. To relate this simulated analysis with practical applications, we fabricated 10/10 nm Pt/Pd@Ag nanoislands (annealed at 200˚C) on alumina substrate and exposed to a certain concentration of hydrogen gas (Fig. 4-16). A maximum amount of 2.3 % response (120˚C) was observed for Pt/Pd@Ag annealed at 200˚C sample case. However, smaller amount of (%) response was observed for other samples which could happen for several factors such as Ag nanoislands diffusion process, Pt/Pd/Ag alloy formation, gaps in nanoparticles. Figure 4-16 shows the hydrogenation and dehydrogenation curves (resistance versus time) for Pt/Pd@Ag nanoislands at 10000 ppm hydrogen at 120℃ temperature for different nanoislands structure. Gradual changes in the base resistance were observed for the different annealed condition of Ag nanoislands (fig.4-13a-e) depending on the nanoislands morphological structure.
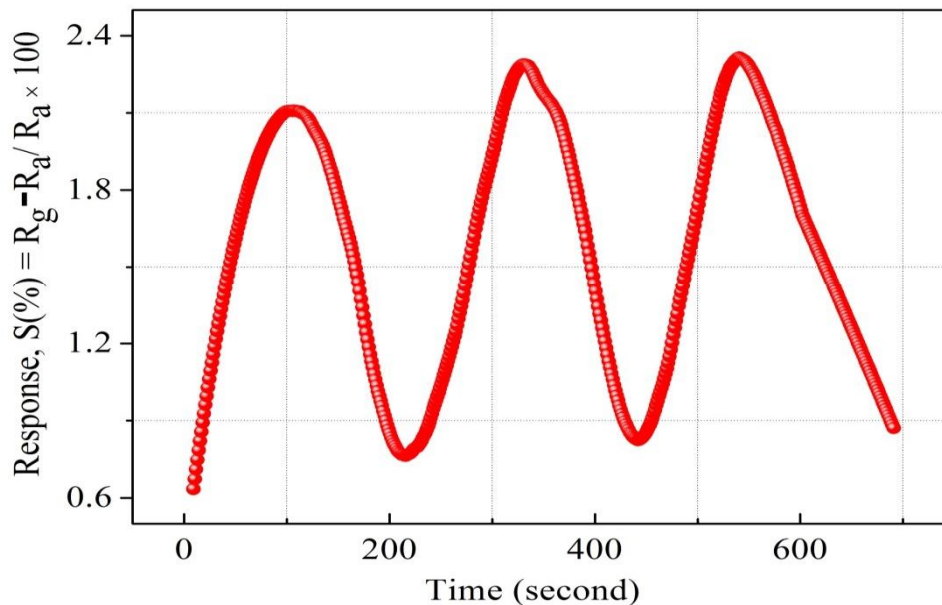
Figure 4-16. Repeatability of S1 at 10000 ppm (120˚C)

The time needed for 90% change in the base resistance after exposing hydrogen gas and the time needed to reach the resistance to its initial value are defined as response and recovery time. A longer time of average 130 sec was measured as response time for Pt/Pd@Ag nanoislands non-annealed sample (labeled as S0) and a sluggish recovery of more than average 160 sec at 120˚C. A lesser amount of catalytic metal alloy interface could be a probable reason for this. However, a faster response time of average 20 sec and recovery of average 25 sec at 120˚C for Pt/Pd@Ag nanoislands annealed at 200˚C sample (labeled as S1), which might be a good and better catalytic metal alloys interfacial effect along with uniform particle distribution. Apart from S1sample, S2, S3, S4 show little delayed response and recovery time (fig. 4-13) along with a lower drift in base resistances depending on the Ag nanoislands morphology. The observations conclude that connectivity between bimetal nanoparticles and metal islands is reducing with the diffusion process induced by annealing temperature. Hence, a less catalytic metal alloy interface and synergetic interplay are occurring which delaying the hydrogen physisorption and chemisorption process. However, for S1 sample case, the interactions of hydrogen molecules with the interstitials sites of catalytic metals alloy scatters the electrons more faster to incorporate hydrogen induced lattice expansion at the ß (metal hydride phase) which eventually shows a faster response time [93]. Along with faster response, a faster recovery time for S1 sample could be due to the higher grains of the interface that can be used as desorption pathway for hydrogen molecules [94]. In addition with the interfacial grains, an optimized temperature of 120˚C was the best fit of electron scattering process as, Pt has higher absorption rate at 100˚C with fast response but lacks in recovery whereas, Pd has slower absorption rate along with high response magnitude and faster recovery [90,91]. Furthermore, catalytic metal alloy of Ag

needs moderate elevated temperature to dissociate the chemisorbed hydrogen molecules [95,66]. A co-operative interaction between the bimetal and metal islands layer induce more tensile stress that helps to dissociate the molecules more [92].So it can be assumed that, at 120˚C both the bimetal and nanoislands metal compete each other and incorporate a faster response and recovery time. Figure 4-17 summarizes the response and recovery at different temperature.
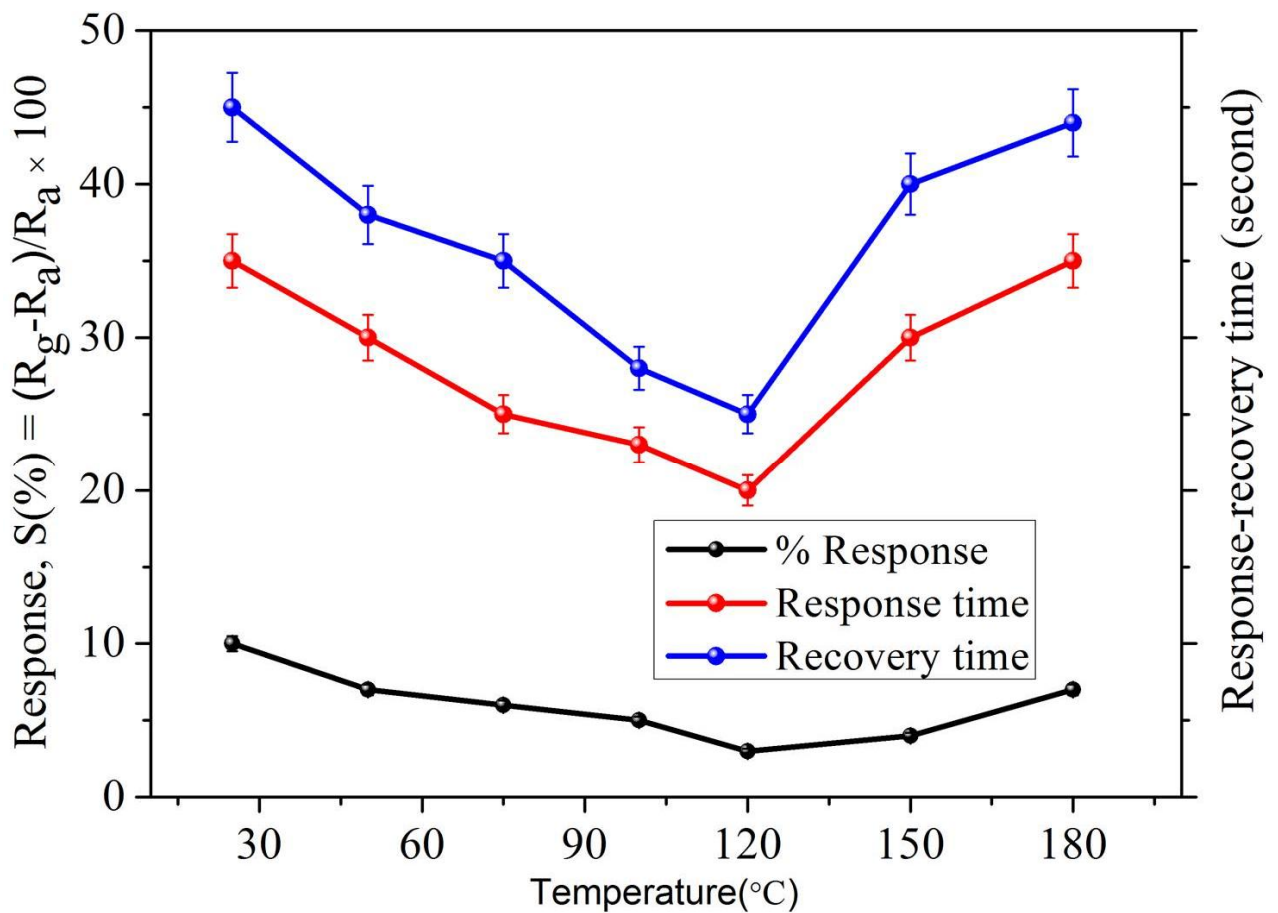
Figure 4-17. Response and recovery at different temperature

The dynamic resistance variation of the as fabricated device were investigated by testing various hydrogen concentration (500 ppm to 400000 ppm) at 120˚C in figure 4-18.
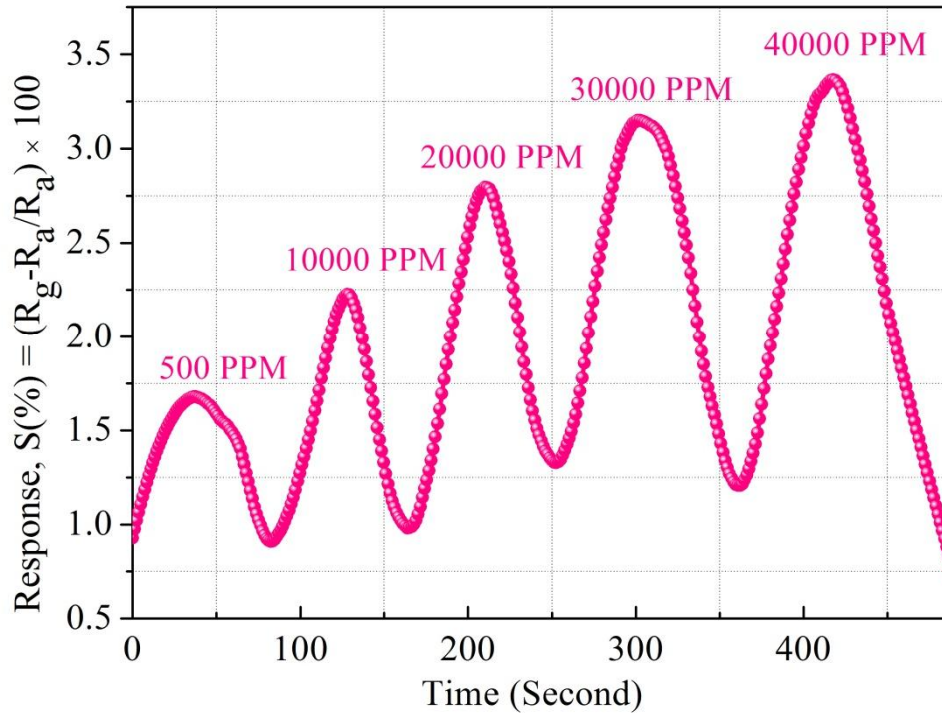
Figure 4-18. Dynamic response

A linear response for wide ranges of hydrogen concentration was found for S1 sample. Hydrogen absorption in Pd materials, such as thin films [93], nanowire [94], nanodisk [95], has shown hysteresis and breaking phenomenon after few cycles of hydrogen absorption whereas, the presently studied Pt/Pd@Ag nanoislands structure performed well at the high concentration of 40000 ppm hydrogen. A negligible hysteresis effect was due the uniform Pt layer which enhances the passing of hydrogen molecules to interact with Pd/Ag alloy along with an increased clamping effect that reveals a tensile stiffness of a laminate specimen is in inverse relation to the thickness of the specimen [96]. The response magnitude for wide ranges of hydrogen concentration was theoretically modeled by Sievert law for S1 sample in figure 4-19, where linearity between the response and the square root of hydrogen concentrations was observed. The linearity confirms that the sample S1 follows Sievert's law.
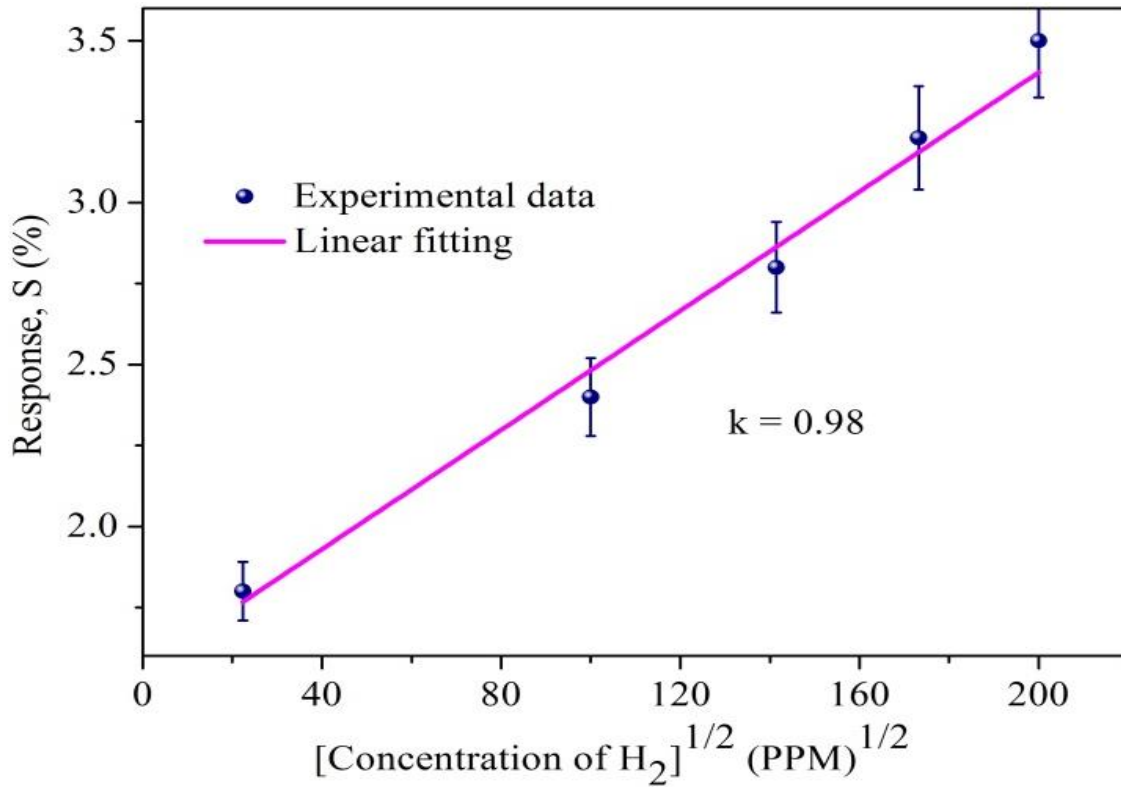
Figure.4-19. Sievert's law for S1 sample

S(%) α √P(H₂), where P(H₂) is the partial pressure of hydrogen. The value of K= 0.98 is the measurement of how close the data are to the fitted regression line.

Hydrogenation of the as-prepared device has the potential of the sensing in real field application, however it can be strongly affected by the presence of water vapor [85, 86]. This can slow down the hydrogenation response by impeding the dissociation of hydrogen molecules on the catalytic metal surface [77, 78, 79]. However, in this work a highly hydrophobic surface having a contact angle of 127.3° (fig. 6f) can create more active sides for hydrogen adsorption by impeding the water vapor. Thus, it creates a greater hydrogenation and dehydrogenation property by increasing the hydrophobicity for quantum size Pt/Pd@Ag nanoislands structure.

4.3. Summary

In this chapter, the effects of thermal annealing surface diffusion on the Ag morphology, and the loading of Pt/Pd bimetal and their catalytic properties towards hydrogenation and dehydrogenation were fully analyzed.

The experimental indicates that that, at 200°C thermally annealed Ag nanoislands (6.50 nm) with an Pt/Pd bimetal of 10/10 nm structure shows enhanced catalytic morphology and fast hydrogenation and dehydrogenation performance .

The main points of this chapter are summarized below:

- ✓ Resistivity type hydrogenation and dehydrogenation properties based on Pt/Pd@Ag nanoislands decorated over alumina substrate is established.

- ✓ By optimizing the Ag nanoislands morphology, the intermetallic catalytic alloy formation with Pt/Pd bimetal enhances.

- ✓ An optimized Pt/Pd (10/10 nm) bimetal enhances the surface charge density which eventually increase the hydrophobicity of the gas absorption surface.

- ✓ A fast response/recovery time of 20/25 sec at a concentration of 10000 ppm H_2 with a response magnitude of 2.3% (120°C) was achieved.

- ✓ Good repeatability and good range of detection (500-40000 ppm H_2) are achieved.

Chapter 5: Conclusions and future works

5.1. Conclusions

In this current study, the hydrogenation and dehydrogenation properties of Pt/Pd bimetal decorated over Ag nanoislands on alumina substrate were studied. Thermally annealing process induced surface diffusion provides a high surface to volume ratio based Ag nano structured islands morphology which provide an enhance catalytic property with Pt/Pd bimetal for the adsorption and desorption of hydrogen molecules at an elevated (120°C) temperature. A response magnitude of 2.3% with a detection range of 500 ppm to 40000 ppm for hydrogen gas was observed with a good repeatability. A fast average response and recovery time of 20/25 sec for 10000 ppm were recorded which also shows high hydrophobicity. We expect that, the as prepared (Pt/Pd@Ag nanoislands) device will be a promising building block for future hydrogen detection technology in hydrogen economy based applications.

5.2. Suggestions for future works

Detecting hydrogen at a wide range with higher stability, selectivity, faster response has intensive research potential. The area of interest can be continued as follows:

- ✓ As the connectivity and alloying between nano sized catalytic metal, plays a very important role for hydrogen absorption, higher surface to volume ratio based template beneath the metal can be designed for increase the hydrogen absorption capability.

- ✓ Optimizing the substrate conductivity and developing high surface to volume ratio

based hierarchical nanostructured catalytic metal can enhance the hydrogenation and dehydrogenation phenomenon.

✓ Developing heterogeneous interfacial structure with 2D conductive material such as Graphene with Pd, Pt can enhance the hydrogen molecules interaction.

5.3. Publications

List of articles published:

First authorship

1. **Rahaman Md Habibur**, Usman yaqoob, Hyeon Cheol Kim, "**Fast hydrogenation and dehydrogenation of Pt/Pd bimetal decorated over nano structured Ag islands grown on alumina substrate**" "**SENSORS" (2.45), in press**

2. **Rahaman Md Habibur**, Usman Yaqoob, Sheeraz Muhammad, Hyeon-Cheol Kim, "The effect of RGO on dielectric and energy harvesting properties of P(VDF-TrFE) matrix by optimizing electroactive β phase without traditional polling process", **Materials chemistry and physics**, **(IF: 2.084).** **https://doi.org/10.1016/j.matchemphys.2018.05.010**.

3. **Rahaman Md Habibur**, Hyeon Cheol Kim, "The Effects of conductive nano filler's nano alignment on the dielectric and energy harvesting properties of co-polymer matrix", **Advanced Manufacturing: Polymer & Composites Science**

Co-authorship

1. Usman Yaqoob, Muhammad Sheeraz, **Rahaman Md Habibur,** Hyeon Cheol Kim, "Realization of self-poled, high performance, flexible piezoelectric energy harvester by employing PDMS-rGO as sandwich layer between P(VDF-TrFE)-PMN-PT composite sheets". **Composite part B**, [IF: 4.72], in press

Conference publications:

First authorship

1. **Rahaman Md Habibur, Hyeon Cheol Kim,** Catalytic Behaviors of Pt/Pd Bimetallic Core-shell Nanoparticles Decorated on Different Basal Podium for Fast Response Hydrogen Sensing, **2017 IEEE SENSORS (SENSORS)**, **Glasgow, Scotland, United Kingdom. IEEE Xplore, DOI:10.1109/ICSENS.2017.8234317**

REFERENCES

[1] Lubitz, W & Tumas, W. Hydrogen: an Overview. *Chem. Rev.* 107, 3900–3903 (2007).

[2] Grochala, W. First Tere was Hydrogen. *Nat. Chem*. **7,** 264–265 (2015).

[3] M.T. Azar, B. Sutapun, R. Petrick, A. Kazemi, Highly sensitive hydrogen sensors using palladium coated fiber optics with exposed cores and evanescent filed interaction, Sens. Actuators B 56 (1999) 158–163.

[4] Karim, G. A. Hydrogen as a spark ignition engine fuel. Int. J. Hydrogen Energy 2003, 28, 569-577

[5] Firth, J. G.Jones, A.Jones, T. A. The principles of the detection of flammable atmospheres by catalytic devices. Combust. Flame 1973, 20, 303-311.

[6] O.K. Varghese, D. Gong, M. Paulose, K.G. Ong, C.A. Grimes, Hydrogen sensing using titania nanotubes, Sens. Actuators B 93 (2003) 338–344.

[7] C.S. Rout, S.H. Krishna, S.R.C. Vivekchand, A. Govindaraj, C.N.R. Rao, Hydrogen and ethanol sensors based on ZnO nanorods, nanowires and nanotubes, Chem. Phys. Lett. 418 (2006) 586–590

[8] B. Wang, L.F. Zhu, Y.H. Yang, N.S. Xu, G.W. Yang, Fabrication of a SnO2 nanowire gas sensor and sensor performance for hydrogen, J. Phys. Chem. C 112 (2008) 6643–6647.

[9] Shegai T, Langhammer C. Hydride formation in single palladium and magnesium nanoparticles studied by nanoplasmonic dark-field scattering spectroscopy. Adv Mater 2011;23:4409e14

[10] Kim JS, Kim BJ. Highly sensitive MEMS-type micro sensor for hydrogen gas detection by modifying the surface morphology of Pd catalytic metal. Kor J Mater. Res 2014;24(10):527e32.

[11] A. Pundt, Hydrogen in nano-sized metals, Adv. Eng. Mater. 6 (2004) 11–22.

[12] F. Yang, D.K. Taggart, R.M. Penner, Fast, sensitive hydrogen gas detection using single palladium nanowires that resist fracture, Nano Lett. 9 (2009) 2177–2182.

[13] P. Offermans, H.D. Tong, C.J.M.V. Rijn, P. Merken, S.H. Brongersma, M.C. Calama, Ultralow-power hydrogen sensing with single palladium nanowires, Appl. Phys. Lett. 94 (2009) 223110.

[14] K.J. Jeon, J.M. Lee, E. Lee, W. Lee, Individual Pd nanowire hydrogen sensors fabricated by electron-beam lithography, Nanotechnology 20 (2009) 135502.

[15] F. Favier, E.C. Walter, M.P. Zach, T. Benter, R.M. Penner, Hydrogen sensors and switches from electrodeposited palladium mesowire arrays, Science 293 (2001) 2227–2231.

[17] Yitian Peng, Jianxin Ye, Lulu Zhenga and Kun Zouab,The hydrogen sensing properties of Pt–Pd/reduced graphene oxide based sensor under different operating conditions, RSC Adv., 2016, 6, 24880.

[18] J. Henriksson, L.G. Villanueva, J. Brugger, Ultra-low power hydrogen sensing based on a palladium-coated nanomechanical beam resonator, Nanoscale 4 (2012) 5059–5064

[19] C.H. Han, D.W. Hong, I.J. Kim, J. Gwak, S.D. Han, K.C. Singh, Synthesis of Pd or Pt/titanate nanotube and its application to catalytic type hydrogen gas sensor, Sens. Actuator, B 128 (2007) 320–325

[20] E. Lee, J.M. Lee, E. Lee, J. –S. Noh, J.H. Joe, B. Jung, W. Lee, Hydrogen gas sensing performance of Pd?Ni alloy thin films, Thin Solid Films 519 (2010) 880–884.

[21] Y. Pak, S.-M. Kim, H. Jeong, C.G. Kang, J.S. Park, H. Song, R. Lee, N.S. Myoung, B.H. Lee, S. Seo, J.T. Kim, G.-Y. Jung, Palladium-decorated hydrogen-gas sensors using periodically aligned graphene nanoribbons, ACS Appl. Mater. Interfaces 6 (2014) 13293–13298.

[22] F. Wu, J.E. Morris, The effect of hydrogen absorption on the electrical

conduction in discontinuous palladium films, Thin Solid Films 246 (1994) 17–23.

[23] S. Bouhtiyya, L. Roue, Pd/Mg/Pd thin films prepared by pulsed laser deposition under different helium pressures, structure and electrochemical hydriding properties, Int. J. Hydrogen Energy 34 (2009) 5778–5784

[24] Y. Liu, M. Chi, V. Mazumder, K.L. More, S. Soled, J.D. Henao, S. Sun, Composition-controlled synthesis of bimetallic PdPt nanoparticles and their electro-oxidation of methanol, Chem. Mater. 23 (2011) 4199–4203.

[25] Offermans, P.; Tong, H. D.; van Rijn, C. J. M.; Merken, P.; Brongersma, S. H.; Crego-Calama, M. Ultralow-Power Hydrogen Sensing with Single Palladium Nanowires. Appl. Phys. Lett. 2009, 94, 223110–223112.

[26] Suleiman, M.; Jisrawi, N. M.; Dankert, O.; Reetz, M. T.; Bähtz, C.; Kirchheim, R.; Pundt, A. Phase Transition and Lattice Expansion during Hydrogen Loading of Nanometer Sized Palladium Clusters. J. Alloys Compd. 2003, 356, 644–648.]

[27] Lee J, Shim W, Lee E, Noh JS, Lee W. Highly mobile palladium thin films on an elastomeric substrate: nanogapbased hydrogen gas sensors. Angew Chem Int Ed 2011;50:5301e5

[28] Favier, F.; Walter, E. C.; Zach, M. P.; Benter, T.; Penner, R. M.Hydrogen Sensors and Switches from ElectrodepositedPalladium Mesowire Arrays. Science 2001, 293, 2227–2231

[29] Walter, E. C.; Favier, F.; Penner, R. M. Palladium MesowireArrays for Fast Hydrogen Sensors and Hydrogen-Actuated
Switches. Anal. Chem. 2002, 74, 1546–1553.LIM ET AL. VOL. 6 ' NO. 1 ' 598–608 ' 2012www.acsnano.org608

[30] Jeon, K. J.; Jeun, M.; Lee, E.; Lee, J. M.; Lee, K. I.; von Allmen,P.; Lee, W. Finite Size Effect on Hydrogen Gas Sensing

Performance in Single Pd Nanowires. Nanotechnology2008, 19, 495501–495506.

[31] Cherevko, S.; Kulyk, N.; Fu, J.; Chung, C.-H. HydrogenSensing Performance of Electro-Deposited Conoidal Palladium Nanowire and Nanotube Arrays. Sens. Actuators B2009, 136, 388–391.

[32] Yang, F.; Taggart, D. K.; Penner, R. M. Fast, SensitiveHydrogen Gas Detection Using Single Palladium Nanowires That Resist Fracture. Nano Lett. 2009, 9, 2177–2182.

[33] Yang, F.; Taggart, D. K.; Penner, R. M. Joule Heating aPalladium Nanowire Sensor for Accelerated Response and
Recovery to Hydrogen Gas. Small 2010, 6, 1422–1429.

[34] Yang, F.; Kung, S.-C.; Cheng, M.; Hemminger, J. C.; Penner,R. M. Smaller is Faster and More Sensitive: The Effect of
Wire Size on the Detection of Hydrogen by Single Palladium Nanowires. ACS Nano 2010, 4, 5233–5244.]

[35] Effects of Pt shell thickness on self-assembly monolayer Pd@Pt core-shell nanocrystals based hydrogen sensing A.S.M. Iftekhar Uddin, Usman Yaqoob, Kamrul Hassan, Gwiy-Sang Chung , j.ijhydene.2016.06.138

[36] Fast-Response Room Temperature Hydrogen Gas Sensors Using
Platinum-Coated Spin-Capable Carbon Nanotubes Daewoong Jung,* Maeum Han, and Gil S. Lee, ACS Appl. Mater. Interfaces 2015, 7, 3050-3057

[37] Fast-Response Room Temperature Hydrogen Gas Sensors Using
Platinum-Coated Spin-Capable Carbon Nanotubes Daewoong Jung,* Maeum Han, and

 Gil S. Lee, ACS Appl. Mater. Interfaces 2015, 7, 3050-3057.

[38] Graham T. On the relation of hydrogen to palladium. In: Proc. of the Royal Society of London, 17; 1868. p. 212e20.

[39] Gryaznov V. Metal containing membranes for the production of ultrapure hydrogen and the recovery of hydrogen isotopes. Sep Purif Methods Rev 2000;29(2):171e87.

[40] Fast-Response Room Temperature Hydrogen Gas Sensors Using Platinum-Coated Spin-Capable Carbon Nanotubes, Daewoong Jung, Maeum Han, and Gil S. Lee, ACS Appl. Mater. Interfaces 2015, 7, 3050-3057

[41] Jiamin quan, Jie Zhang, Xueqiang Qi, Junying Li, Ning Wang, Yong Zhu, A study on the corre;lation between the dewetting temperature of Ag film and SERS intensity, SCIENTIFIC REPORTS, 2017-11-07.

[42] Rota, A. *et al*. Au island growth on a si(1 1 1) vicinal surface. *Surf. Sci.* 600, 1207–1212 (2016).

[43] Rufno, F., Cacciato, G. & Grimaldi, M. G. Surface difusion coefcient of au atoms on single layer graphene grown on cu. J. Appl. Phys. 115, 666 (2014).

[44] Jiran, E. & Tompson, C. V. Capillary instabilities in thin flms. *J. Electron. Mater.* **19**, 1153–1160 (1990).

[45] Jiran, E. & Tompson, C. V. Capillary instabilities in thin flms. *J. Electron. Mater.* **19**, 1153–1160 (1990).

[46] Liu, L. *et al*. Slow gold adatom difusion on graphene: efect of silicon dioxide and hexagonal boron nitride substrates. *J. Phys. Chem. B* **117**, 4305 (2013).

[47] Rha, J. J. & Park, J. K. Stability of the grain confgurations of thin flms—a model for agglomeration. *J. Appl. Phys.* **82**, 1608–1616 (1997)

[48] Huang, C. W. *et al*. Surface-enhanced raman scattering of suspended monolayer graphene. *Nanoscale Res. Lett.* **82**, 480 (2013).

[49] Qiu, C., Zhou, H., Cao, B., Sun, L. & Yu, T. Raman spectroscopy of morphology-controlled deposition of au on graphene. *Carbon* **59**, 487–494 (2013)

[50] Zhang, J. *et al*. Ag-cu nanoparticles encaptured by graphene with magnetron sputtering and cvd for surface-enhanced raman scattering. *Plasmonics* **11**, 1495–1504 (2016)

[51] Mo, Y. W., Kleiner, J., Webb, M. B. & Lagally, M. G. Activation energy for surface difusion of si on si(001): a scanning-tunnelingmicroscopy study. *Phys. Rev. Lett.* **66**,

1998 (1991)

[52] Kim, H. C., Alford, T. L. & Allee, D. R. Tickness dependence on the thermal stability of silver thin flms. *Appl. Phys. Lett.* **81**, 4287–4289 (2002)

[53] Duyne, R. P. V., Hulteen, J. C. & Treichel, D. A. Atomic force microscopy and surface-enhanced raman spectroscopy. i. ag island flms and ag flm over polymer nanosphere surfaces supported on glass. *J. Chem. Phys.* **99**, 2101–2115 (1993).

[54] S.M. Chiu, S.J. Hwang, C.W. Chu, D. Gan, The influence of Cr-based coating on the adhesion force between epoxy molding compounds and IC encapsulation mold, Thin Solid Films 515 (2006) 285–292.

[55] Owens, D.K. and Wendt, R.c.; Jour. Applied polymer Sci., 13, 1741, (1969).

[56] M. Yamauchi, H. Kobayashi, H. Kitagawa, Hydrogen storage mediated by Pd and Pt nanoparticles, Chem. Phys. Chem. 10 (2009) 2566–2576

[57] An X-ray diffraction study of interface roughness and diffusion in Ag/Pd superlattices, Thin Solid Films 342 (1999) 174–179, K. Temsta,*, M.J. Van Baela, C. Van Haesendoncka, Y. Bruynseraedea, D.G. de Grootb,N. Koemanb, R. Griessenb

[58] Davoud Dorranian, Shiva Tajmir, Farzane Khazanehfar Effect of Laser Fluence on the Characteristics of Ag Nanoparticles Produced by Laser Ablation, *Soft Nanoscience Letters*, 2013, 3, 93-100

[59] Mohamed A. Salem, Eman A. Bakr, Heba G. El-Attar, Pt@Ag and Pd@Ag core/shell nanoparticles for catalytic degradation of Congo red in aqueous solutionSpectrochimica Acta Part A: Molecular and Biomolecular Spectroscopy (2017) j.saa.2017.07.002

[60] Synthesis and structural investigation of Pd/Ag bimetallic nanoparticles prepared by the solvothermal method, Journal of Nanoparticle Research (2007) 9:1153–1161, 11051-006-9203-5

[61] M. Zhang, Y. Li, Z. Yan, J. Jing, J. Xie, M. Chen, Electrochim. Acta 158 (2015) 81–88

[62] E. Alfonso, J. Olaya, G. Cubillos, Thin Film Growth Through Sputtering Technique and

Its Application, INTECH Open Access Publisher, 2012

[63] Li Y, Wang ZW, Chiu CY, Ruan L, Yang W, Yang Y, et al. Synthesis of bimetallic Pt-Pd core-shell nanocrystals and their high electrocatalytic activity modulated by Pd shell thickness. Nanoscale 2012;4:845e51.

[64] Liu X, Xu G, Chen Y, Lu T, Tang Y, Xing W. A strategy for fabricating porous PdNi@ Pt core-shell nanostructures and their enhanced activity and durability for the methanol electrooxidation. Sci Rep 2015;5:6.

[65] Lee J, Shim W, Lee E, Noh JS, Lee W. Highly mobile palladium thin films on an elastomeric substrate: nanogapbased hydrogen gas sensors. Angew Chem Int Ed 2011;50:5301e5

[66] H. Takagi, H. Ogawa, Y. Yamazaki, A. Ishizaki and T. Nakagiri, Quantum size effects on photoluminescence in ultrafine Si particles, Appl. Phys. Lett. 56 (1990) 2379.

[67] H. Morisaki, F. W. Ping, H. Ono and K. Yazawa, Above-band-gap photoluminescence from Si fine particles with oxide shell J. Appl. Phys. 70 (1991) 1869.

[68] H. Morisaki , Above-band-gap photoluminescence from Si fine particles Nanotechnol. 3 (1992) 196

[69] H.-S. Chen, J.-J. Chiu and T.-P. Perng,On THE PHOTOLUMINESCENCE OF Si NANOPARTICLES, Mater.Phys.Mech. 4 (2001) 62-66

[70] R. Zakaria, K.S. Hamdan, S.M. Che Noh, A. Supangat and M. Sookhakian, Surface plasmon resonance and photoluminescence studies of Au and Ag micro-flowers, Optical Materials Express, 10.1364/OME.5.000943.

[71] Y. Zhao, Y. Jiang, and Y. Fang, "Spectroscopy property of ag nanoparticles," Spectrochim. Acta A Mol. Biomol. Spectrosc. **65**(5), 1003–1006 (2006).

[72] T. Suna, Z. Xua, W. Zhaoa, X. Wua, S. Liua, Z. Zhanga, S. Wanga, W. Liua, S. Liub, and J. Peng, "Fabrication of the similar porous alumina silicon template for soft uv nanoimprint lithography," Appl. Surf. Sci. **276**, 363–368 (2013).

[73] Wadell C, Syrenova S, Langhammer C. Plasmonic hydrogen sensing with nanostructured metal hydrides. ACS Nano 2014;8:11925e40

[74] Yang F, Kung SC, Taggart DK, Penner RM. Hydrogen sensing with a single palladium nanowires. Sens Lett 2010

[75] Yang F, Donavan KC, Kung SC, Penner RM. The surface scattering-based detection of hydrogen in air using a platinum nanowire. Nano Lett 2012

[76] Gland JL, Sexton BA, Fisher GB. Oxygen interactions with the Pt (111) surface. Surf Sci 1980.

[77] Fisher GB, Gland JL. The interaction of water with the Pt (111) surface. Surf Sci 1980

[78] obayashi H, Yamauchi M, Kitagawa H, Kubota Y, Kato K, Takata M. Hydrogen absorption in the core/shell interface of Pd/Pt nanoparticles. J Am Chem Soc 2008.

[79] P.F. Ruths, S. Ashok, S.J. Fonash, J.M. Ruths, A study of Pd/Si MIS schottky barrier diode hydrogen detector IEEE trans, Electron Devices 28 (1981) 1003–1009

[80] Li X, Liu Y, Hemminger JC, Penner RM. Catalytically activated palladium@platinum nanowires for accelerated hydrogen gas detection. ACS Nano 2015;9:3215-25.

[81] J.L. Gland, B.A. Sexton, G.B. Fisher, Oxygen interactions with the Pt (111) surface, Surf. Sci. 95 (1980) 587–602

[82] G.B. Fisher, J.L. Gland, The interaction of water with the Pt (111) surface, Surf. Sci. 94 (1980) 446–455.

[83] M. Johansson, L. Ekedahl, Hydrogen adsorbed on palladium during water formation studied with palladium membranes, Appl. Surf. Sci. 173 (2001)122–133

[84] Pd/Ag alloy as an application for hydrogen sensing, Bharat Sharma, Jung-Sik Kim, Department of Materials Science and Engineering, University of Seoul, Seoul 02504, South Korea, IJHE, 2017.08.142

[85] MEMS based highly sensitive dual FET gas sensor using graphene decorated Pd-Ag alloy nanoparticles for H2 detection, Bharat Sharma & Jung-Sik Kim, Scientific REPORTS. (2018) 8:5902

[86] Yitian Peng, Jianxin Ye, Lulu Zhenga and Kun Zouab,The hydrogen sensing properties of Pt–Pd/reduced graphene oxide based sensor under different operating conditions, RSC Adv., 2016, 6, 24880

[87] K. Hassan et al. Fast-response hydrogen sensors based on discrete Pt/Pd bimetallic ultra-thin films, Sensors and Actuators B 234 (2016) 435–445

[88] X.-Q. Zeng, Y.-L. Wang, H. Deng, M.L. Latimer, Z.-L. Xiao, J. Pearson, T. Xu, H.-H.Wang, U. Welp, G.W. Crabtree, W.-K. Kwok, Networks of ultrasmall Pd/Cr nanowires as high performance hydrogen sensors, ACS Nano 5 (2011) 7443–7452

[89] Yang F, Donavan KC, Kung SC, Penner RM. The surface scattering-based detection of hydrogen in air using a platinum nanowire. Nano Lett 2012;12:2924-30.

[90] A.S.M. Iftekhar Uddin, Usman Yaqoob, Kamrul Hassan, Gwiy-Sang Chung, Effects of Pt shell thickness on self-assembly monolayer Pd@Pt core-shell nanocrystals based hydrogen sensing, j.ijhydene.2016.06.138

[91] K Yoshimura1, S Nakano2, S Uchinashi3, S Yamaura4, H Kimura4 and A Inoue4, A hydrogen sensor based on Mg–Pd alloy thin film, Meas. Sci. Technol. **18** (2007) 3335–3338

[92] E. Lee, J.M. Lee, E. Lee, J.-S. Noh, J.H. Joe, B. Jung, et al., Hydrogen gas sensing performance of Pd–Ni alloy thin films, Thin Solid Films 519 (2010) 880–884.

[93] F. Yang, D.K. Taggart, R.M. Penner, Fast, sensitive hydrogen gas detection using single palladium nanowires that resist fracture, Nano Lett. 9 (2009) 2177–2182.

[94] C. Langhammer, I. Zoric, B. Kasemo, B.M. Clemens, Hydrogen storage in Pd nanodisks characterized with a novel nanoplasmonic sensing scheme, Nano Lett. 7 (2007) 3122–3127.

[95] K.I. Lundstrom, M.S. Shivaraman, C.M. Svensson, A hydrogen sensitive Pd-gate MOS transistor, J. Appl. Phys. 46 (9) (1975) 3876–3881

[96] K.I. Lundstrom, M.S. Shivaraman, C.M. Svensson, A hydrogen sensitive Pd-gate MOS transistor, J. Appl. Phys. 46 (9) (1975) 3876–3881.

APPENDIX – CHARACTERIZATION

A.1 Evaluation methods for materials characterization

The surface morphologies of Ag nanoparticles on alumina substrate at different annealing conditions were analyzed using field emission scanning electron microscopy (FESEM; JEOL JSM JEM – 7600F). Nano structured Ag nanoislands roughness and RMS grain size was checked in 3D atomic force microscopy (AFM). Water droplet contact angles were measured by contact angle goniometry (Kruss DSA 100 drop shape analyzer) using the sessile drop method at room temperature. Distilled deionized water droplets (about 3 μL) were dropped on the thin film surfaces using a micro-syringe. Pt/Pd bimetal and their nanostructured discrete thin film distribution were studied with a JEOL JEM-2010F energy dispersive spectrometer (EDS). The structural properties were investigated using an X-ray diffractometer (XRD, Rigaku Ultima IV) with Cu Kα ($\lambda = 0.154$ nm) radiation over a 2θ scanning range of 10-90˚. The chemical compositions were checked by X-ray photoelectron spectroscopy (XPS) using Al Kα radiation as the X-ray source. Photo-luminescence (PL) spectra were obtained on a perkin Elmer LS 55 setup. A keithely probes station was used for measuring the resistance changes of the as prepared devices.

A.2 Evaluation methods for sensing measurement hydrogenation and dehydrogenation measurement:

The as prepared device was mounted inside of a chamber, and a keithly probe station (SCS-4200) with a bias voltage fixed at 1 V was used to check the ohmic conduction and resistance. A computerized mass flow controller (ATOVAC, GMC 1200) system was used to change the concentration of H_2 gas in synthetic air (Deokyang Co., Ltd).Gas mixture with different H_2 concentrations were delivered to the chamber at a constant flow rate of 200

standard cubic centimeters per minute (sccm). The gas chamber was supplied with synthetic air between each H_2 pulse to allow the device surface to return to atmospheric conditions. The gas concentration was controlled and measured using the following equation;

$$\text{Desiredgas}_{con.} \text{ (ppm)} = \frac{\text{Flowrate}_{gas}}{\text{Flowrate}_{gas} + \text{Flowrate}_{syntheticair}} \times \text{Suppliedgas}_{con.} \text{ (ppm)}$$

The sensor response was defined as;

$$S, (\%) = \frac{R_g - R_a}{R_a} \times 100$$

Where R_g and R_a is the resistances of the sensor in hydrogen gas exposure and air exposure at certain concentrations, respectively. The response and recovery time of the as prepared device was defined as the time taken to reach 90% of the total resistance change.